Electronic supplementary:

The onset of ecological diversification 50 years after colonisation of a crater lake by haplochromine cichlid fish

Appendix S1: Methods: Fish sampling

Gill nets were set at various depths in the benthic habitat in Lake Chala. The few nets (4 times three joined nets with 16, 19 and 22mm mesh size) that we set in the limnetic habitat remained empty. For each gill net, the depth was measured and recorded with the use of sinkers. Fish were carefully removed from the net and photographed from their left side in a custom designed photo cuvette with a colour reference bar, a scale bar and a standardized grey background. The fish was afterwards sacrificed with an overdose of phenoxyethanol diluted in lake water. From the right side of each fish, we removed the pectoral fin and kept it in pure analytical ethanol (100%) for DNA extractions, and we removed a piece of the epaxial muscle dorsal of the lateral line, removed the skin, and dried the muscle tissue in an oven (60°C for 24 to 48 hours) for stable isotope analysis. Whole fish were subsequently fixed in 4% formalin (buffered with borax) and were later rinsed with water and stepwise transferred to 75% ethanol.

In addition to *Astatotilapia*, we sampled all other fish species occurring in Lake Chala (*Oreochromis hunteri*, *O. sp*. 'blue head' and *Coptodon rendalli*) using the methods described above. Additionally we bought several larger *O. hunteri* from a local fisherman on the lake, who was fishing by hook and line. We also sampled *Astatotilapia cf. bloyeti* from the nearby Nyumba ya Mungu Reservoir (bought from the market), a dammed reservoir in the Ruvu/Pangani River, and *Astatotilapia sp.* from Lake Babati (gill netting), and *Oreochromis spp.* from the Nyumba ya Mungu (fish market), the Ruvu River (angling) and Lake Babati (gill netting) to reconstruct the colonization history of Lake Chala cichlids.

Appendix S2: Methods: Filtering procedure for the RAD-tag sequences

Raw reads (100 bp each) for the genomic analyses came from six libraries. Each library resulted in between 175 mio and 290 mio raw reads. Sites were filtered to include only reads with an intact *Sbf*I restriction site, de-multiplexed and barcode-trimmed (to a length of 90 bp) using stacks and the FASTX toolkit v.0.0.13. Afterwards, reads with at least 5% of the bases with a quality below 30 were excluded for every individual with the FASTX toolkit v.0.0.13.

The remaining reads were mapped against the reference genome of *Metriaclima zebra* (1) for phylogenetic analyses, F-statistics and STRUCTURE-analyses, and against the reference genome of *Oreochromis niloticus* (2) for F-statistics, PCA and STRUCTURE analyses. We used two different reference genomes to retain as many SNPs as possible for the phylogenetic analyses, while getting chromosomal information for the genome scans and F-statistics. Base quality scores for the mapped reads were recalibrated using empirical error rate estimations that we gained from bacteriophage PhiX reads (3). Genotypes were called with the GATK tool UnifiedGenotyper and filtered for genotype depth (>20), genotype quality (>30), maximal allowed missing data of 50% per site and indels were removed using vcftools (4). We removed all individuals with more than 50% missing data using vcftools. This dataset was used as the basis for all subsequent analyses. Below, additional filtering steps are indicated for each analysis separately.

RAxML v8.0.0 (5) was used to build a maximum likelihood tree using all concatenated sequences (~2 Mio sites, including monormorphic and polymorphic sites). For each of 100 bootstrap replicates, we resampled sites from the concatenated dataset. From each

resampled dataset, the maximum likelihood tree was inferred using a GTRGAMMA model. Bootstrap support was then calculated based on these 100 topologies and was plotted on the edges of the best-scoring maximum-likelihood tree calculated from the complete data set.
For STRUCTURE analyses we extracted all individuals from Lake Chala (N = 90) and additionally removed all monomorphic and all multiallelic sites, applied a more stringent missing data filter (maximally 20% missing data allowed per site) and applied a minor allele count cut-off of 3 (assuring that all alleles occurred in at least two individuals). This resulted in a vcf-file with 1,239 SNPs for the alignment to *M. zebra* and a vcf-file with 545 SNPs for the alignment to *O. niloticus*. For the genomic PCA we used the same file but applied an additional minor allele frequency cut-off of 2% resulting in 514 SNPs in the overall analyses and 466 – 522 SNPs for the pairwise analyses.
From the vcf-file that we used for the STRUCTURE-analyses, we extracted all possible morph-pairs to calculate F-statistics. After extracting these pairs, we further excluded all sites that were not at least sequenced for two individuals of both morphs in each pair, resulting in between 1,013 and 1,187 SNPs (for *M. zebra* and 462 – 522 SNPs for *O. niloticus*). Because Weir and Cockerham's F-Statistics are highly influenced by sample sizes (small sample sizes *per se* and different sample sizes between the two populations; (6)), we additionally subsampled for each morph pair genotypes within each morph to equal sample sizes. For this, we randomly subsampled a certain number (K) of genotypes for each genomic site. Thereby creating "fake" individuals that have alleles mixed from all individuals of the same morph. The resulting dataset has identical sample sizes for all morphs, but still contains the whole variation originally present within each morph. For each pair of morphs K=N-1 genotypes (where N represents the sample size of the less common morph) were subsampled 50 times. For each subsampling we calculated F-statistics in vcf-tools (4). We report the mean of the 50 weighted F_{ST} values of the 50 subsampling events in table S13.
To ask whether these F_{ST}s between phenotypically defined morphs were higher than expected by chance when sampling from the Lake Chala population, we performed a permutation test with 100 permutations. We subsampled 100 times the same number (2*K+2) of individuals from all our 90 sequences of Lake Chala *Astatotilapia* and randomly assigned them to two groups with equal sample sizes (K+1). For each permutation we used one of these subsampled datasets. In each permutation both populations were subsampled to K genotypes (as described before) 50 times and weighted F_{ST}s calculated for each of these subsampling events. The average of these 50 F_{ST}s was used as one permutation. Subsequently we used the fraction of these 100 permutations that reached higher average weighted F_{ST}s than the observed average in our data, as a measure of significance of the observed F_{ST}.

Appendix S3: Methods: Demographic modelling
For the demographic modelling, we used individuals of *Astatotilapia cf. bloyeti* from the Pangani River (riverine, Nyumba ya Mungu and the Mkuzi River), *Astatotilapia sp.* from Lake Chala (LC) and *Pundamilia pundamilia* (PPM) and *P. nyererei* (PNM) from Makobe Island in Lake Victoria. Individuals with insufficient sequence data (more than 66% missing data and/or evidence for excessive PCR-duplication) were excluded. This dataset was filtered for maximally 50% missing data per site and maximally 66% missing data per individual. In order to exclude paralogous sites, we removed sites with mean sequencing depth of more than 150 across all sequenced individuals (average mean site depth of 48.0) and sites with a heterozygosity excess with a p-value below 0.001 (HWE test with vcftools).
Then we subsampled at each nucleotide site 10 randomly chosen genotypes per population (except for the riverine population that we subsampled to 5 genotypes per site because we

only had sequencing data from 8 individuals). With these data we calculated multidimensional site frequency spectra (SFS) in Arlequin v. 3.5 (7), which we used for the demographic modelling in fastsimcoal2.6 (8). As we do not know the derived or ancestral state of the alleles, we computed minor allele SFS. The fit of each model to the observed SFS was maximized using the composite-likelihood method implemented in fastsimcoal2.6 (5). For each run, we performed 100,000 coalescent simulations (-N) with 40 expectation-maximization (EM) cycles (-L 40), using 0.001 as minimum relative difference in parameter values for the stopping criterion (-M). Only SFS entries above 5 were taken into account for the parameter estimations because low entry categories cannot be estimated precisely (-C). We used wide search ranges with log-uniform distributions for all model parameters (table S6). For each model, we performed 100 independent fastsimcoal2.6 runs and retained the run with the highest maximum likelihood.

Overall we ran 3 x 8 models. We estimated the splitting time between the *Astatotilapia sp.* of Lake Chala and the *Astatotilapia cf. bloyeti* of the Pangani River under four different scenarios, each combined either with a simple split followed by isolation or with a later admixture event (simulating an additional colonization event, see figure S3). The four different scenarios consisted of the Lake Chala population modelled either with a) constant population size from colonization to now, b) a bottleneck directly after colonization, followed by recovery but no continuous expansion, c) a continues expansion starting directly after colonization and continuing till now, or d) a bottleneck directly after colonization, followed by a recovery and expansion that continues till today (figure S3, for the parameters check table S6).

In the first 8 models, which we term “mutation rates models”, we dated the divergence of the Chala from the river population using the published mutation rate of 3.5×10^{-9} mutations per generation estimated in Malinsky et al. (9). In the other 2x8 models, we dated divergence of the Chala population from the river population by fixing one other older splitting time with well constrained age. We used two different divergence events to have two independent estimates for the age of the Lake Chala population. First, we ran all models fixing the split-time between Lake Victoria *Pundamilia* (representative of any Lake Victoria Region Superflock member) and riverine *Astatotilapia* at 3 Mio generations (as estimated in (10) assuming a generation time of 2 years). We subsequently refer to these models as “three population models”. Second, we ran all 8 models fixing the splitting time between the two Lake Victoria endemics *Pundamilia pundamilia* and *Pundamilia nyererei* to 6’000 generations (corresponding to the time in generations when Lake Victoria filled up after several thousand years of complete desiccation, following Meier et al., 2017). We subsequently refer to these models as “four population models”. Both divergence events that we fixed in time are conservative with regard to testing the hypothesis that the colonization of Lake Chala was recent: The 6’000 generations fixed in the “four population models” represent the refilling event of Lake Victoria but it is rather unlikely, that the two *Pundamilia* species split from each other immediately upon the colonization of the lake by the ancestors of all 500 endemic Lake Victoria cichlid species. The 6 Mio years (~3 Mio generations) that we used as a split time between the Lake Victoria Region Superflock members (represented by *Pundamilia*) and *Astatotilapia bloyeti* in the “three population models” is the upper end of the range estimated in Meier et al., 2017 (1.7 to 6 Mio years). Both divergence events happened, therefore, likely more recently than the time we fixed. Consequently, we most likely overestimate the separation-time between the *Astatotilapia* of Lake Chala and those of the Pangani River, but do not underestimate it.

Appendix S4: Methods: ABBA-BABA tests of introgression

Several *Oreochromis* species (*O. esculentus, O. niloticus*) from the Lake Victoria catchment were introduced to the Pangani River. To test whether also haplochromines of the Lake Victoria Region may have been translocated to Lake Chala, we performed tests of introgression (ABBA-BABA tests) with ADMIXTOOLS 1.1 1 (11). Using *Astatotilapia cf. bloyeti* or *A. sparsidens* as sister group to *A. sp*. 'Chala', and *Metriaclima zebra* as outgroup, we tested for excess allele sharing indicative of gene flow between *A. sp*. 'Chala' with either Lake Victoria Region Superflock (LVRS) or *H. gracilior*. To test if more than one of the NE Tanzanian river haplochromine species colonized Lake Chala, we used the same test with either *A. bloyeti* from the Pangani, *A. cf. bloyeti* from the Ruaha Swamps further south in Tanzania, or *A. sparsidens* from Lake Manyara as sister group to *A*. *sp*. 'Chala' to look for excess allele sharing with the other one respectively.

Appendix S5: Methods: Test for morphospace expansion in Lake Chala

To test whether *Astatotilapia sp.* 'Chala' expanded their realized morphospace, compared to its closest known relative outside Lake Chala, we performed a PCA over both populations (Lake Chala and Nyumba ya Mungu) and compared the area that each community occupies in the shared morphospace. To account for differences in allometry between the two populations, we did a slightly different size correction than the one we used for analyses for Lake Chala only. We ran an ANCOVA with lake and SL as covariates for each log transformed morphometric trait. Then we used the standardized residuals of each trait after removing lake effects. These residuals were used for the PCA and all subsequent analyses comparing *Astatotilapia* from Lake Chala with *Astatotilapia cf. bloyeti* from Nyumba ya Mungu. We also calculated the area of the convex hull, and used it as an indicator of realized morphospace for both populations. Because we only had 10 fish from Nyumba ya Mungu, we resampled (1000 times) both populations to a sample size of nine individuals, calculated the area of their convex hull (chull-function in the R-package grDevices) and compared average permutated hull size between the two populations using a t-test.

To test for a range expansion of single morphometric traits, we performed Levene tests for each trait (leveneTest-function in the R-package car). As the power of Leven decreases with inequality of samples sizes, we additionally subsampled 10 Lake Chala *Astatotilapia* and compared their trait range with the trait range observed for *Astatotilapia cf. bloyeti* from Nyumba ya Mungu.

Appendix S6: Methods: Colour analyses

We defined eight regions on the fish body that are important for differentiation in nuptial coloration among closely related species of haplochromine cichlids (12) or seemed particularly variable within the *Astatotilapia* of Lake Chala (figure S1). Fins were excluded from colour analyses because fins were not fully opened on all pictures. We assigned one of eleven colours to each region of the fish body (table S3). These colours were assigned to two colour categories (table S4) representing the two most distinct colour morphs found in Lake Chala (blue and yellow, figure S1 B and C).

Because colour intensity changes rapidly with the motivational state of fish and fades away quickly after capture, we run all analyses which include our colour measurements twice. Once, where we only included individuals that do not show any evidence of colouration change after capture (N=84, figure 2) and once we included all individuals where we were certain that we still could assign the proper colour for every of the eight regions on the fish body (N=127, figure S10A). The results for both datasets are very similar.

Appendix S7: Methods: Stable isotope and stomach content analyses

For stable isotope analyses, dried muscle tissue was ground into fine powder using a QIAGEN Tissuelyzer II with five-millimetre stainless steel beads (QIAGEN). Of this powder, 0.25 - 0.35 mg was used to analyse $\delta^{13}C$ and $\delta^{15}N$ values in a ThermoFisher Scientific Flash 2000 elemental analyser coupled through a Conflo IV interphase to a Delta V Advantage Isotope Ratio Mass Spectrometer (IRMS). To test whether the $\delta^{13}C$ signature changes along the depth gradient (which would confirm that the fish were caught were they actually forage) and to test whether the different morphs differ in single stable isotopic signatures, we conducted ANOVAs. Additionally, to test whether the different morphs explain more variation in the stable isotope signature than depth alone we conducted an ANCOVA with stable isotopes ($\delta^{13}C$ and $\delta^{15}N$) as response variable and depth and morph as predictors.

To further investigate into the trophic ecology of *Astatotilapia* in Lake Chala, we dissected the stomachs of 140 fish. Stomach contents were analysed by quantifying volumetric proportions (13) of 13 prey types. Fish with an empty or almost empty stomach (less than 25% full) and fish that were not assigned to a morph were excluded from further analyses, resulting in 59 analysed stomachs. We then calculated Schoener's index of diet-overlap to assess prey item differences between morphs.

Appendix S8: Methods: Fitness proxy

Scale circuli are deposited on regular intervals and therefore can be used as an age-estimator (14-17). For 231 individuals of *Astatotilapia sp.* 'Chala', we collected ontogenetic scales from the first row above the lateral line, cleaned them in a supersonic water bath and photographed them on microscope slides with a Leica camera (DFC290HD) mounted on a Leica MZ12 microscope. These pictures were used to count the number of circuli along one of the most central grooves on the anterior part of the scale in tpsDig2 (18). Our fitness proxy was estimated by using the standardized residuals of the linear regression between the number of circuli and log-transformed SL. Therefore, it is not representing growth rate per se, but rather the deviation of an individual's growth rate from the expected population-wide growth rate. This method has been validated with an experiment in van Rijssel et al. (19).

Appendix S9: Methods: Selection analyses

Beside the well-established methods described in Lande and Arnold (20), which takes into account correlation between morphological traits, we additionally tested each trait independently for its relationship to our fitness proxy. Therefore, we calculated linear, quadratic and polynomial models. To evaluate which model fits our data best, we quantified the relative model fit using the Akaike Information Criterion (21) with a small-sample-size correction (AICc). We considered the next complex model as a better fit, if AICc decreased by at least 2.5. Correlational selection between traits was tested using the glm function in R. These regression coefficients have to be interpreted with caution as they may reflect either selection or selection gradients.

Appendix S10: Methods: Depth categories

Depth categories were defined such as to represent a light, well-oxygenated (~ 8 mg L^{-1}) shallow water habitat (0-7.5m water depth), an intermediate depth habitat around the oxycline where dissolved oxygen concentrations drop down to 6 mg L^{-1} (8-25 m depth) and an oxygen-poor (< 6mg L^{-1}), profundal habitat (> 25.5 m). Temperature and oxygen measurements were taken from Damste et al (22). To test whether the trait combinations

under strongest selection change between these three depth categories, we calculated depth-specific PPR on individuals of each depth category separately, leading to depth-specific eigenvalues, and used those to create depth-specific fitness surfaces.

Appendix S11: Methods: Fitness surface changes between different depth categories
To test whether the differences among the fitness surfaces for the different depth categories were significant, we performed paired Wilcoxon signed rank tests for the estimated fitness values between the fitness surfaces. For these analyses we only used the morphospace which was in the range of a1 and a2 values covered by all five depth categories. In the resulting morphospace we generated a grid with 50x50 cells (N=2500) so that the grids perfectly match each other for the different fitness surfaces (Schema matching). In the paired Wilcoxon signed rank test, we compared the estimated fitness values for each of these 2500 cells between two different surfaces of the different depth categories. A visual representation of the relationship between the estimated fitness surfaces for the same point in morphospace is in figure S21.
Additionally, to test whether taking depth into account for estimating the smoothed fitness surfaces improves the model fit, we used generalized additive models calculated in the R-package mgcv (23). We used our raw growth rate measurements as a response variable and a1 and a2 from the Projection Pursuit Regression as predictors including a tensor product interaction and a thin plate spleen smoothing parameter. We compared this model with a model where we additionally included a tensor product interaction with water depth. Models were compared using the Akaike Information Criterion (AIC). The results are shown in figure S22.

Appendix S12: Methods: Evolutionary response
To test for evolutionary response to the selection that might result from the inferred fitness surfaces, we tested i) whether individuals cluster in beneficial (high fitness) areas of the fitness surfaces, and ii) whether individuals of the same morph aggregate at the same side of the fitness valleys. The first was tested by comparing the average predicted fitness ("height" of the fitness surface) at the locations in morphospace where the sampled fish occurred, with the average predicted fitness of randomly distributed individuals in morphospace. We then performed a permutation test (1000 iterations) where we randomly placed individuals on the previously estimated fitness surfaces (assign random a1- and a2-values within the observed range) and calculated the average predicted fitness of all individuals. Hence, we tested whether the observed average predicted fitness is higher than the average predicted fitness if individuals where randomly distributed in the fitness surface by using permutation tests.
To test whether the relative abundance of one morph on one side of the fitness valley was higher than expected by chance, we also performed a permutation test (1000 iterations) where we randomly assigned individuals to morphs. These expected abundances were then compared to the observed abundances to get significance levels. For this analysis, we only included morphs that were present with more than three individuals per analysis (overall, shallow depth habitat, intermediate depth habitat and deep habitat).

Appendix S13: Results: Mitochondrial haplotypes in Lake Chala
Sequences of the mitochondrial D-Loop of *Astatotilapia* from Lake Chala revealed two clearly distinct haplotypes (separated by five mutations in 830 bp). The more common haplotype is also shared with *Astatotilapia bloyeti* from the Mkuzi River, *Astatotilapia* from Lake Babati, and with *Astatotilapia* from the Ruaha swamp-region, and has previously been reported for Lake Chala and Ngare Nanyuki (not shown, because only 355 bp are published; 51). The rarer

Chala haplotype is closely related to another known haplotype from the Mkuzi River (figure 1A).

The D-loop haplotype network for the *Oreochromis* revealed that the endemic *O. hunteri* is most closely related to the geographically nearby Pangani-system endemics, *O. jipe* and *O. pangani*, but does not share any haplotypes with either of these (24). This confirms earlier morphology-based suggestions, that these three species form a "Pangani system flock" of closely related species (25). All haplotypes of *Oreochromis sp.* 'blue head' of Lake Chala, are shared with fish of a similar phenotype that we caught in the upper Pangani (Ruvu River, 24). In *O. sp.* 'blue head' we found two very distinct haplotype groups that differ by 12 mutations (in 355 bp). The only haplotype from GenBank being close to one of these two haplotypes (five mutations apart), is a sequence of *O. urolepis* from the Rufiji River in southern Tanzania. All *Coptodon* that we collected in Lake Chala and in Nyumba ya Mungu share one haplotype, which is slightly different (two mutations away) from the haplotypes of *C. rendalli* from Zimbabwe on GenBank (figure S4)(26).

Appendix S14: Results: Demographic modelling
The best model among the eight tested "mutation rate models" suggests a very recent split between the *Astatotilapia* from Lake Chala and the *Astatotilapia* from Nyumba ya Mungu only 36 generations ago. Further, a bottleneck with less than ten individuals and a very recent second colonization event seems to improve the model fit (table S6, figure S3).
The best model among the eight tested "three population models" suggests that the Lake Chala *Astatotilapia* diverged from the Pangani River *Astatotilapia* less than 50 generations ago (highlighted in red in figure S3). Neither a bottleneck, an expansion, a combination of both, nor a second colonization/admixture event improved the model fit. Among the "four population models" a constant expansion of the Lake Chala population after the splitting time from *Astatotilapia cf. bloyeti* from the Pangani River approximately 270 generations ago slightly improves the model-fit (highlighted in green in figure S3). All models estimated a very recent (less than 275 generations ago) split of *Astatotilapia* of Lake Chala from its ancestors in the Pangani River. Together with the reports from the fishermen and previous fisheries reports (27, 28) they add evidence, that we here indeed describe a haplochromine cichlid population few generations after the colonization of an adaptive zone.

Appendix 15: Results: Male nuptial coloration
The PCA on colour traits revealed three distinct clusters in male colour space (figure 2). One cluster contains all individuals of the morphs PLR, OSH, YBE and most of LEO, representing the yellow colour type (figure S2C) with a yellowish ventral side and head, and a coppery to orange colour on the shoulder and/or dorsum. A cluster with a blueish head, a lightly coloured ventral side and a coppery dorsum contains individuals of PLB and approximately half of BBE and LEA. The third cluster with a blueish head, dark ventral side and purplish dorsum (figure S2B) contains all individuals of GAL and LMO and the other approximate half of BBE and LEA.

Appendix S16: Results: Bivariate and canonical analyses
In our bivariate analyses, we found significant correlational selection on six trait pairs. Four pairs showed stabilizing selection and two of them directional selection, whereas there was no evidence for disruptive selection (table S14, figure S18). The canonical analyses on multiple traits combined revealed no significant disruptive selection either, but three trait combinations under directional and another three under stabilizing selection (table S15).

Appendix S17: Results: Rugged fitness surfaces in the shallow and in the deep habitat

Looking for the trait combinations most strongly associated with fitness variation in the different water depth habitats by calculating separate projections for three depth categories, revealed that different trait combinations were associated with alternative fitness optima at different water depths (figure S25). The most rugged fitness landscape was found in the shallow habitat (γ=0.826), followed by the deep habitat (γ=0.480). The intermediate depth habitat was characterized by a less rugged fitness landscape (γ=0.139, Appendix S16, figure S25). In the shallow habitat, the PPR revealed a fitness surface with two optima along a1 (+SnL, -SnW, +POW and –HL, 5^{th} degree polynomial, $P < 0.001$, table S16+S17, figure S25). In this depth habitat individuals tend to cluster around the optima (figure S23). Consistent with the analyses based on all *Astatotilapia* of Lake Chala (across the entire depth range), GAL is highly overrepresented on the less populated optimum and underrepresented on the other optimum. Further, OSH is underrepresented on the less populated optimum (table S18).

In the deep habitat, PPR revealed a fitness surface with two optima along a1 (+HL, -PPL, -EyD, -BD, +LJW, table S16+S17, figure S25), with LEA being underrepresented on the less populated optimum. Interestingly, most of the traits loading heavily on a1 can be associated with adaptation towards zooplanktivory. And the direction of the loadings fits these predictions. Individuals with $a1 < 0$ would represent the zooplanktivorous type with short heads, large eyes, long premaxillary pedicels and narrow lower jaws.

Appendix S18: Discussion: The colonization history of Lake Chala

Based on mtDNA, previous studies reported that *Astatotilapia sp*. 'Chala' is very closely related to the *Astatotilapia cf. bloyeti* in Ngare Nanyuki, on the Eastern flank of Mount Meru (fig. 1, 29). However, the two waterbodies are neither connected, nor do they share economically interesting fish, which could have explained either recent migration or accidental stocking. Our data, mtDNA and genome-wide RAD sequencing, suggests a close relationship to the *Astatotilapia cf. bloyeti* of the Ruvu/Pangani River. We found a second, less common haplotype within *Astatotilapia sp*. 'Chala', which differs from the more common haplotype by five mutations (in 830 bp). Assuming that *Astatotilapia* arrived in Lake Chala only in the 1970s (27, 30), both haplotypes must have been introduced. We found both haplotypes also in Nyumba ya Mungu, a hydropower reservoir in the Pangani River. Therefore, the Ruvu/Pangani River, and the reservoir that was created when the Nyumba ya Mungu dam was closed in 1965, seems the most likely source population for the colonization of Lake Chala.

Consistent with cichlid introductions from the upper Pangani are also the phylogeographic relationships of the two other introduced cichlid species of Lake Chala. *Oreochromis sp.* 'blue head' shares its two very distinct haplotypes exclusively with *Oreochromis* of similar phenotype that we collected in the Ruvu River, one of the two main inlet rivers of Nyumba ya Mungu. One of these two haplotypes suggests a close relationship to *O. urolepis* from the Rufiji River, but is distinct from the known Rufiji haplotype by five or six mutations (out of 355bp). As the second haplotype is distinct by twelve additional mutations and not closely related to any known *Oreochromis* species, the origin and the evolutionary relationship of *O. sp*. 'blue head' remains unresolved.

Coptodon rendalli from Lake Chala also shares its haplotype with *C. rendalli* from Nyumba ya Mungu (figure S4). Therefore, an accidental introduction of *Astatotilapia* from the upper Pangani as a bycatch of *Oreochromis* or *Coptodon* that were introduced to Lake Chala during the early 1970s seems the most plausible explanation for the arrival of *Astatotilapia* in Lake Chala.

One of our three approaches in the demographic modelling (the "mutation rate models") supports a strong bottleneck and an additional, extremely recent, second colonization event. It thus might be possible that our most distinct fish might have arrived at different colonization events. The two distinct mitochondrial haplotypes detected in *Astatotilapia* of Lake Chala might therefore represent different colonization events. Testing for phenotypic and nuclear genomic differentiation between the two haplotype groups revealed no significant genomic differentiation ($F_{ST} < 0.0001$) and the different haplotypes were randomly distributed in a PCA based on our morphological data. As we also assigned the nine individuals with the rarer haplotypes to five different morphs (and 1 unassigned), it is unlikely that the pattern found in this study might be driven by such an additional, recent colonization event.

Appendix S19: Discussion: Morphological changes associated with novel niches in Lake Chala
Since the colonisation of the lake, *Astatotilapia* invaded the entire well-oxygenated depth range in Lake Chala and expanded in phenotypic traits compared to their putative founder population in the Nyumba ya Mungu reservoir. However, they did not colonize the open water of the pelagic zone. Whereas a shift in mean and range occurred in LJW and EyL, an expansion of the realized trait value range occurred for HW, BD, SnL, IOW, EyD and POW. The same pattern of an expansion in phenotypic trait space was detected in a multivariate analysis, where the *Astatotilapia* of Lake Chala cover a significantly broader range than their relatives in Nyumba ya Mungu. Generally we found that *Astatotilapia* in Lake Chala have a reduced head and body width and larger eyes than the population in the Pangani reservoir (NYM). Given that most of the width measurements were negatively correlated with water depth in Lake Chala (smaller width in the deeper habitat), this could reflect rapid adaptation to requirements in deeper water. Similar trends are observed in the cichlids of Lake Victoria where deep-dwelling genera (e.g. *Pundamilia, Lithochromis*) tend to have more narrow heads (e.g. LJW, IOW, SnW), than shallow-dwelling genera (e.g. *Neochromis, Mbipia*) (31). Large eyes were associated with relatively low $\delta^{15}N$ values, which was associated with the two most zooplanktivorous morphs. As the occurrence of zooplankton in the stomachs of *Astatotilapia* sp. 'Chala' was significantly positively correlated with water depth, the larger eyes in the zooplanktivorous morphs might reflect the larger dependence on zooplankton in deeper, less productive habitats (see also Appendix S16). Several other studies in a broad range of fish species identified better vision and more slender body shape as morphological adaptations to zooplanktivory (31-34).

Appendix S20: Discussion: Divergence in syntopy
Morphological differentiation between morphs mainly involves head width (HW), body depth (BD), lower jaw length (LJL), snout length (SnL) and snout width (SnW). HW and SnW are strongly negatively correlated with lake depth (deep living fish have narrower heads and snouts). Lower jaw length is highly negatively correlated with $\delta^{13}C$, indicating variation along the littoral/profundal feeding axis, and divergence in BD between different morphs gives indications of benthic/limnetic variation (GAL and LMO are deeper bodied, therefore potentially more benthic). Together this provides evidence for divergence along two axes well known to be important for pairwise ecotype formation in fish (35-38).
The most distinct morph of *Astatotilapia sp*. 'Chala' is what we called "Gaurochromis-like" (GAL) because of superficial similarity with the Lake Victoria cichlid genus *Gaurochromis.* It is distinct from all other morphs but one in morphology. Further, this morph is highly overrepresented on an otherwise sparsely occupied optimum on the phenotypic fitness surface (short snouts and small cheek depth), confirming its morphological distinctiveness.

Interestingly, the other morph that is morphologically distinct from all but one other morph is Orange-Shoulder (OSH), which has a very similar water depth distribution to GAL. OSH is strongly differentiated from GAL not only in morphology, but also in male nuptial coloration and feeding ecology ($\delta^{13}C$). In addition, OSH is the morph that is closest to the larger fitness peak (positive a1-values) in the fitness surface (the fitness peak where GAL is highly underrepresented, figure 3). Taken together, this indicates that morph differentiation does not happen exclusively along the depth gradient, but also within a depth habitat.

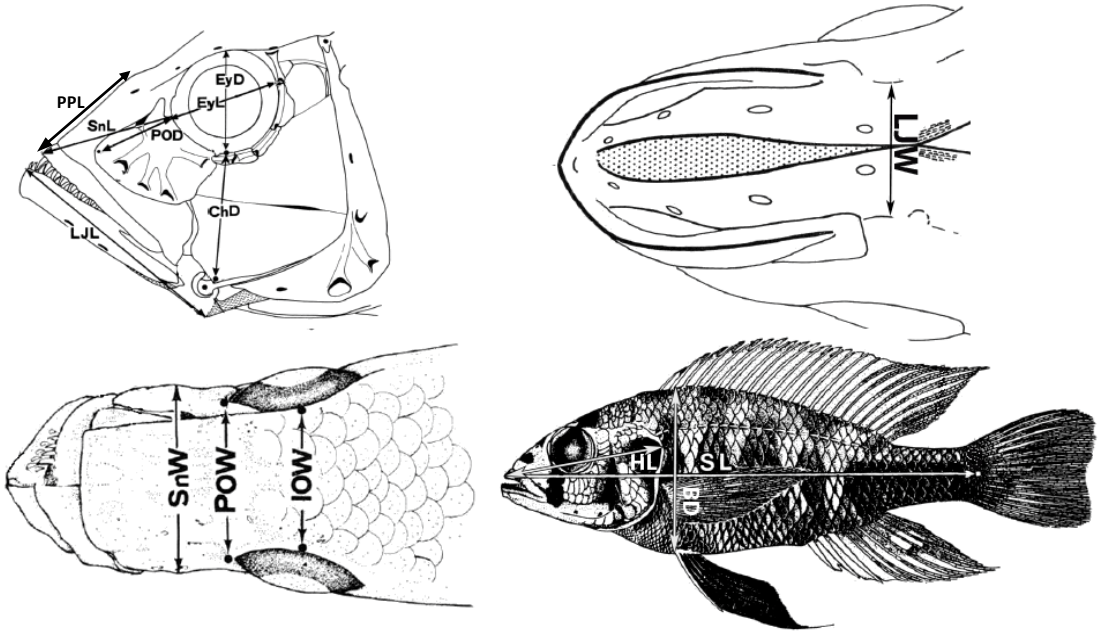


Figure S1: Linear morphometric measurements used in this study. Figure adapted from Barel et al.(39). Note that head width (HW) is not indicated in this figure which is the width between the most caudal point of the left and right operculum, also used to measure head length (HL).

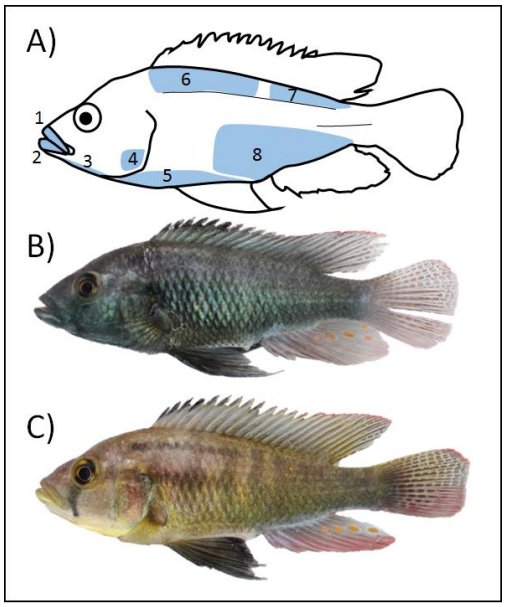


Figure S2: A) Schematic drawing of *Astatotilapia sp.* 'Chala' with the areas considered for colour scoring (1 = upper lip, 2 = lower lip, 3 = branchyostegal membrane, 4 = suboperculum, 5 = belly, 6 = rostral dorsum, 7 = caudal dorsum, 8 = flank) and representatives of the two most distinct colour types; mainly blue (B) and mainly yellow (C).

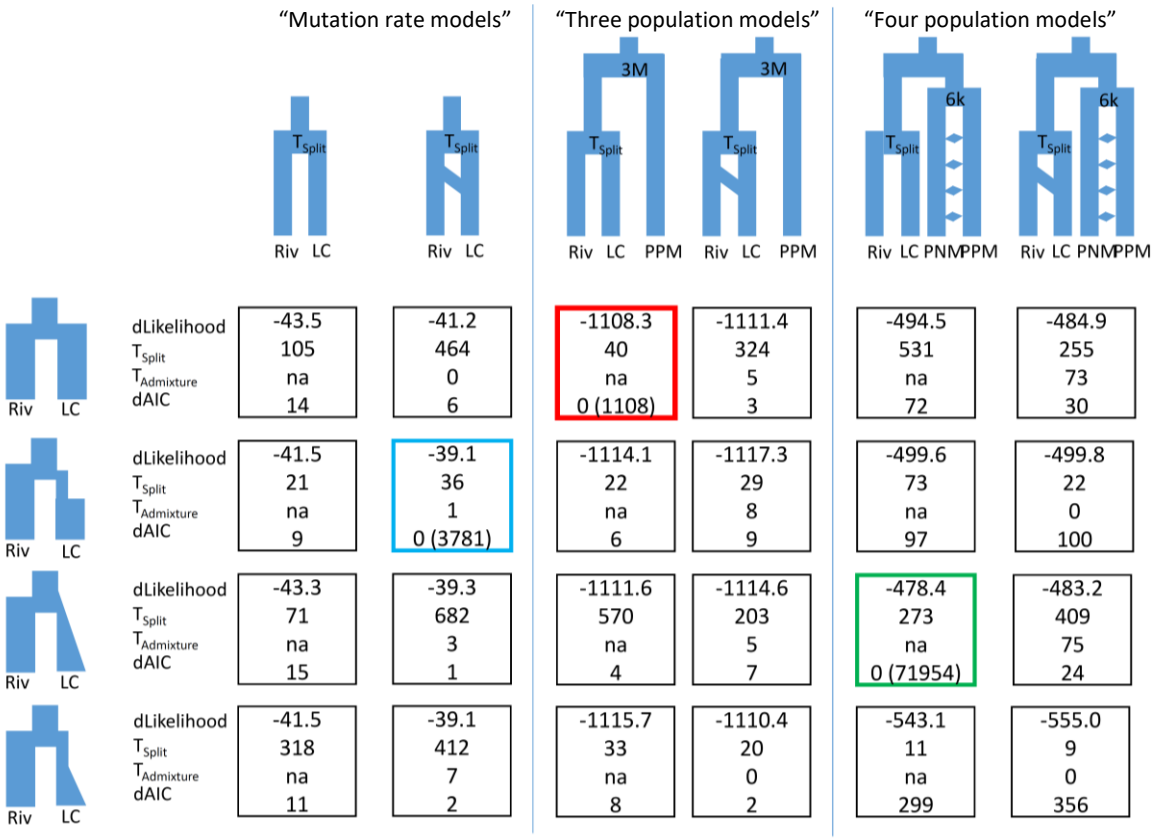


Figure S3: Demographic modelling revealed that the splitting event (T_{Split}) between *Astatotilapia* of Lake Chala (LC) and *Astatotilapia cf. bloyeti* of the Pangani River (Riv) happened very recently. We tested four different scenarios (schematic figures on the left), whereby Lake Chala was either modelled with (from top to bottom) a) constant population size, b) a bottleneck directly after colonization, followed by a recovery, c) a continuous expansion starting directly after colonization and continuing till now, or d) a bottleneck directly after colonization, followed by a recovery and continuous expansion that continues till today (for the parameters check table S6). Each model was tested either with a simple split between Lake Chala and the Pangani *Astatotilapia* (columns 1,3 and 5) or with a second colonization and admixture event (column 2,4 and 6). We dated divergence of the Chala population from the river population using three different and complementary approaches, either using the mutation rate reported for *Astatotilapia calliptera* (columns 1 and 2, "Mutation rate models") in Malinsky et al. (9) or by fixing the time of an older splitting event with well constrained age in the outgroup. For the latter we used two different divergence events: First, we fixed the split-time between Lake Victoria *Pundamilia* (representative of LVRS) and riverine *Astatotilapia* at 3 Mio generations (column 3 and 4, "three population model", (10)). Second, we fixed the splitting time between the two Lake Victoria endemics *Pundamilia pundamilia* and *Pundamilia nyererei* to 6'000 generations (column 5 and 6, "four population models", (40)). For each model we report the delta-likelihood (observed likelihood – estimated likelihood), the estimated split time between Riv and LC (T_{Split}), the estimated time of a second colonization event ($T_{Admixture}$) and the deltaAIC-value (AIC of the best model minus AIC of the reported model). The models with the best fit to the observed data (highest likelihood and lowest AIC, framed in blue, red and green) suggest that *Astatotilapia* sp. 'Chala' split from their ancestors in the Pangani River very recently (36, 40 resp. 273 generations ago), and that there either was just a single colonization event, or a second colonization event occurred extremely recently.

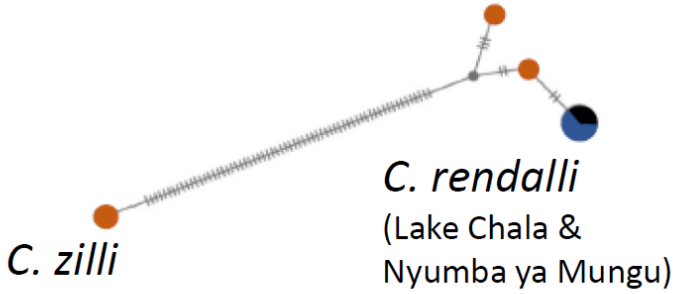


Figure S4: The phylogeographic relationships of *Coptodon rendalli* of Lake Chala. TCS haplotype network (mitochondrial D-loop, 355 bp) for *Coptodon* of Lake Chala (blue), the Nyumba ya Mungu Reservoir (black) and from GenBank (orange)(26, 41). We only used 355 bp (instead of 830 for *Astatotilapia*) because the sequences that we downloaded from GenBank were restricted to this shorter fragment. The size of the circles indicates the number of individuals with a given haplotype in our data, ticks between the circles indicate single point mutations. The corresponding haplotype network for the *Oreochromis spp*. can be found in (24).

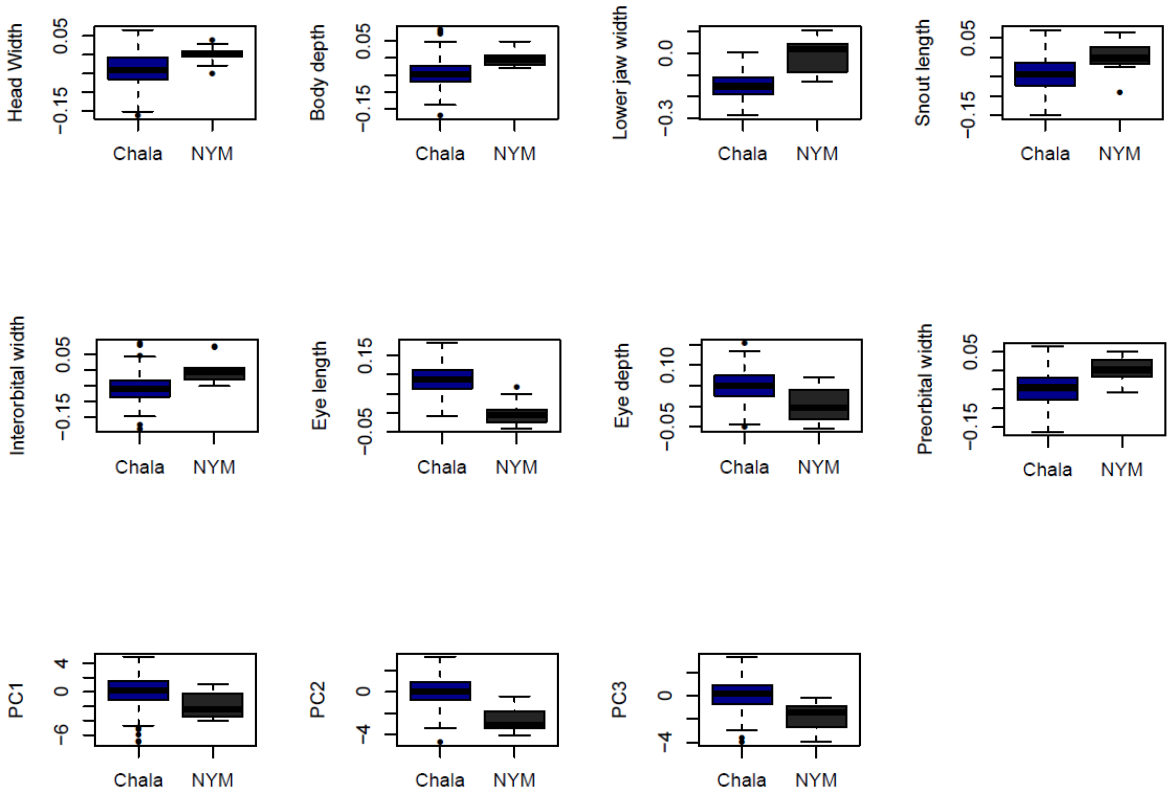


Figure S5: Boxplots of the eight morphological traits that differ significantly (after sequential Bonferroni correction) between *Astatotilapia* from Lake Chala and its closest known relative, *Astatotilapia cf. bloyeti* from the Nyumba ya Mungu reservoir (NYM). The last three plots show the differences between the two populations for the first three PC axes, which are significantly differentiated between the two populations.

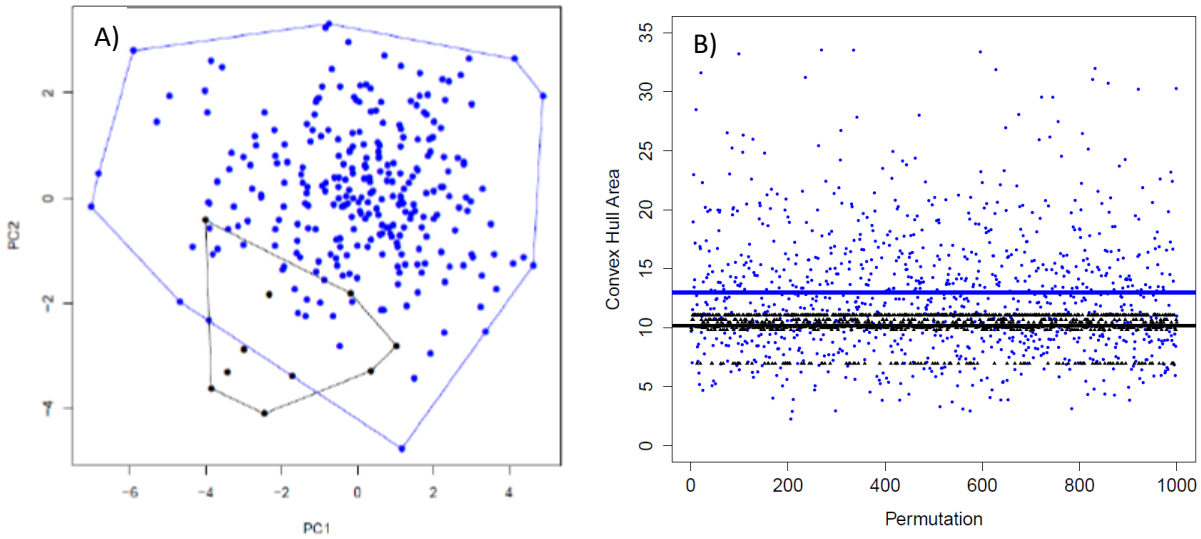
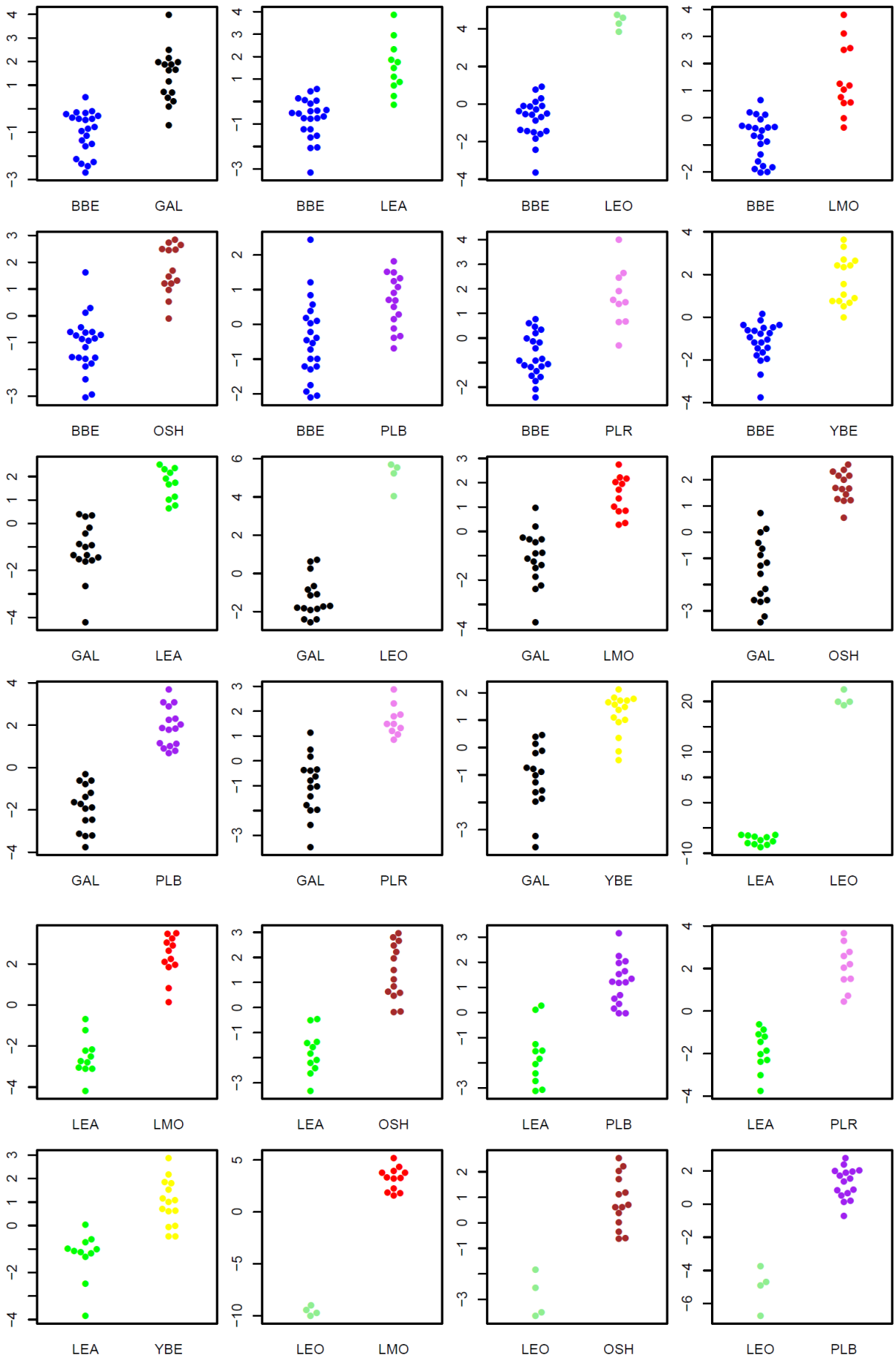


Figure S6: Morphospace occupancy in *Astatotilapia* from Lake Chala (blue) and *Astatotilapia cf. bloyeti* from Nyumba ya Mungu (black) A) indicated as the convex hulls in the morphospace spanning the first two principle components, and B) indicated as the hull sizes (y-axes) of 1000 subsamplings of nine *Astatotilapia sp.* 'Chala'. The blue, upper horizontal line represents the average permutated hull size for nine *Astatotilapia sp.* 'Chala' (13.0) whereas the black, lower line indicates the average permutated hull size for nine *Astatotilapia cf. bloyeti* from Nyumba ya Mungu (10.2). The differences in the permutated hull sizes were highly significant (t-test: $P < 0.001$).


BBE GAL
BBE LEA
BBE LEO
BBE LMO
BBE OSH
BBE PLB
BBE PLR
BBE YBE
GAL LEA
GAL LEO
GAL LMO
GAL OSH
GAL PLB
GAL PLR
GAL YBE
LEA LEO
LEA LMO
LEA OSH
LEA PLB
LEA PLR
LEA YBE
LEO LMO
LEO OSH
LEO PLB

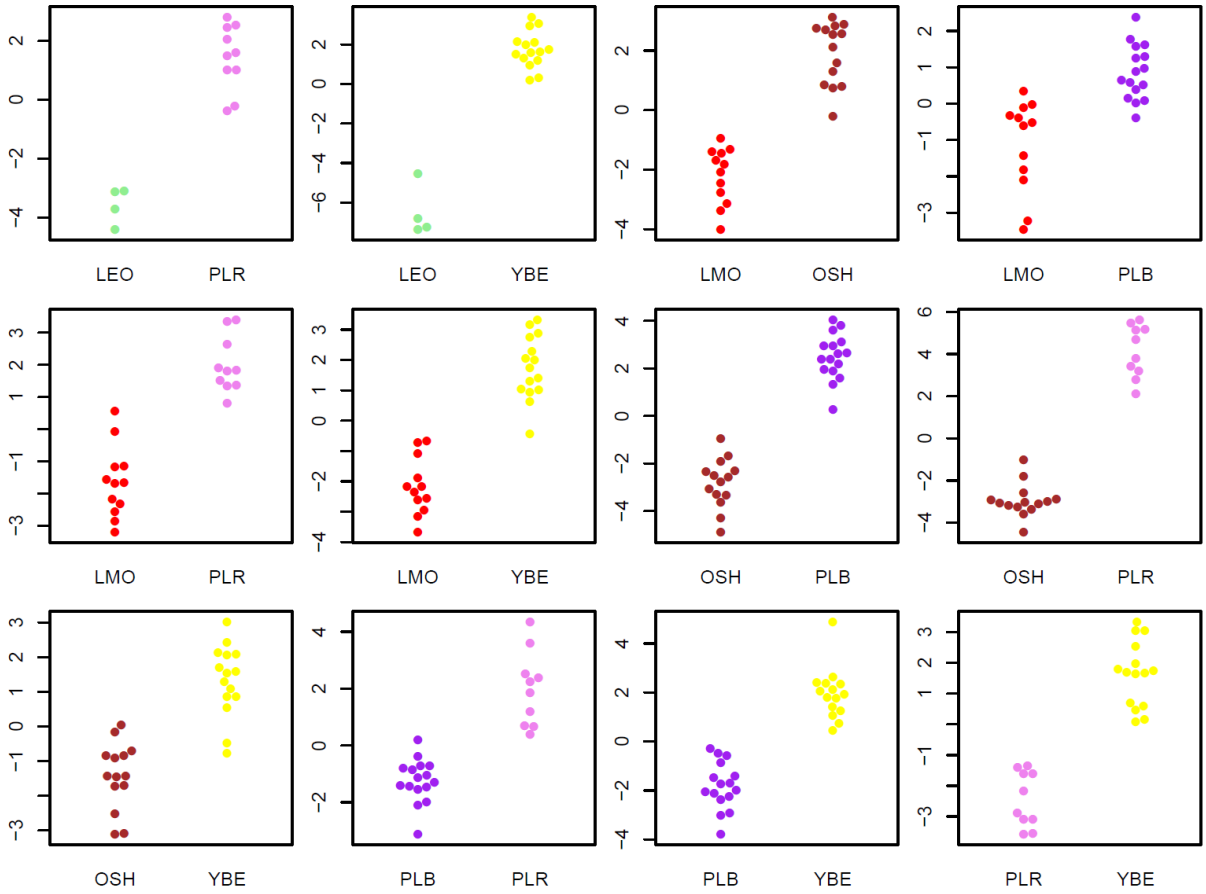


Figure S7: Morphological differentiation of morphs based on pairwise LDA (LD1 on the y-axes). All comparisons were highly significant ($p<0.0011$). Colours correspond to the colours assigned to each morph throughout the manuscript (blue = BBE, black = GAL, green = LEA, light green = LEO, brown = OSH, purple = PLB, violet = PLR, yellow = YBE).

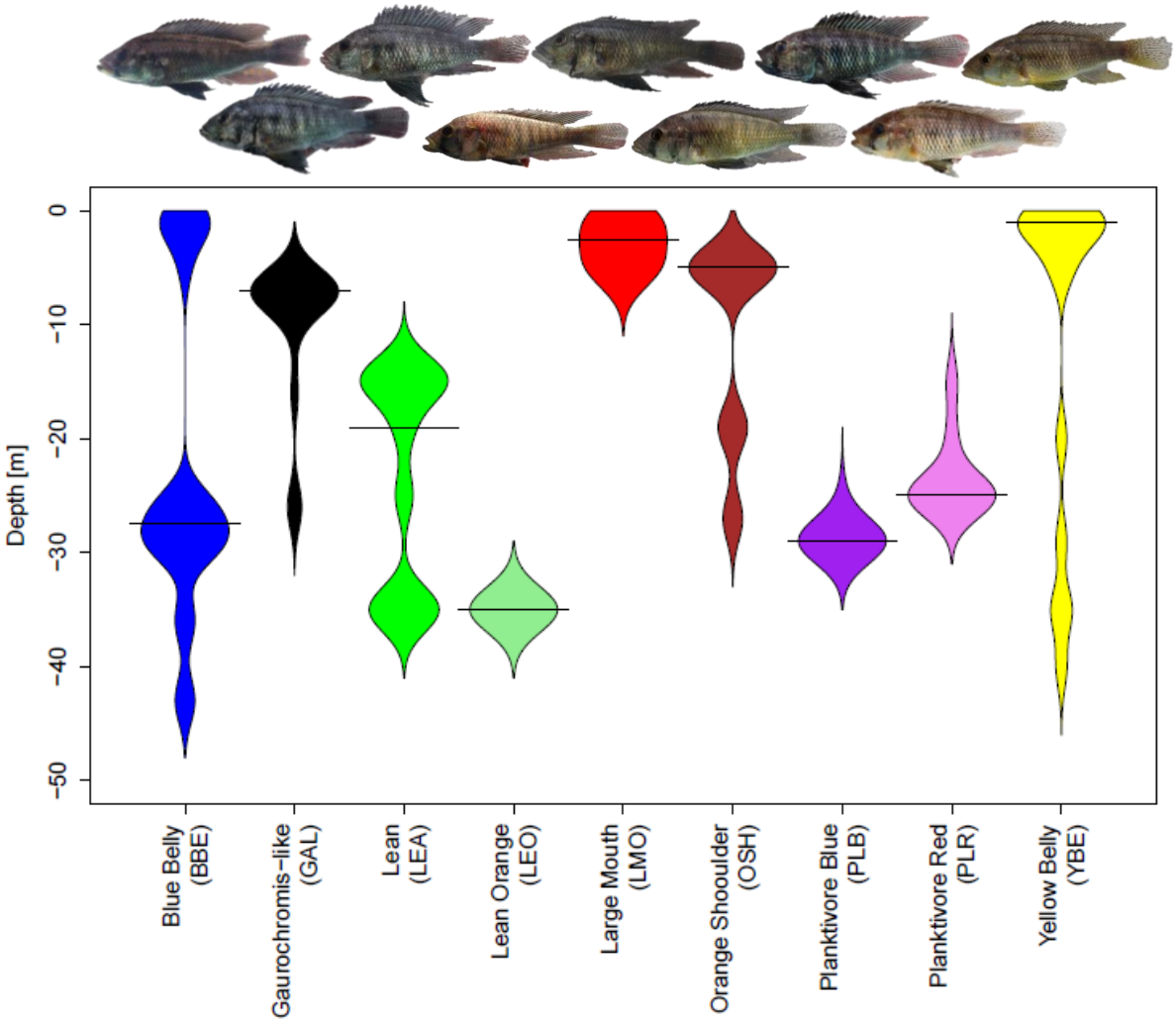


Figure S8: Bean plot of depth utilization for each morph. Horizontal lines represent medians. Differences in depth range occupancy of the different morphs was highly significant (ANOVA: $F = 8.47$, $P < 0.0001$).

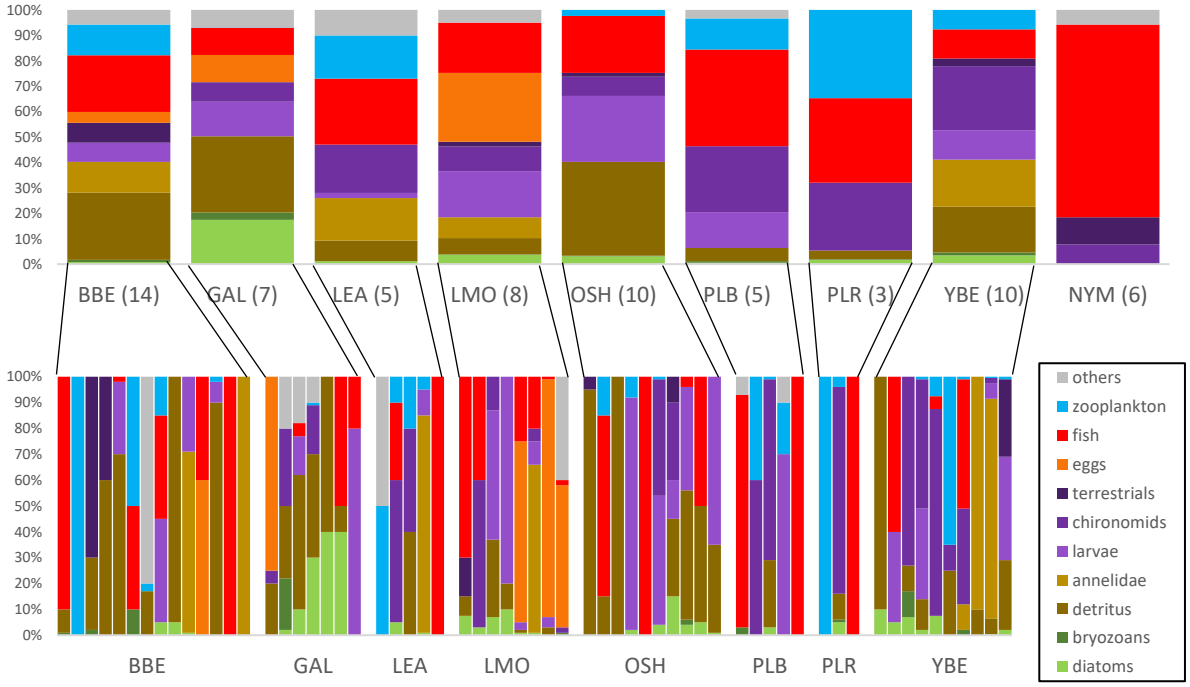


Figure S9: Volumetric proportions of different prey items in the stomachs of *Astatotilapia* of different morphs (upper row) and the corresponding individuals (lower row). Sample sizes are given in the brackets for each morph. The last bar represents stomach contents form *Astatotilapia cf. bloyeti* from the upper Pangani (Nyumba ya Mungu, NYM).

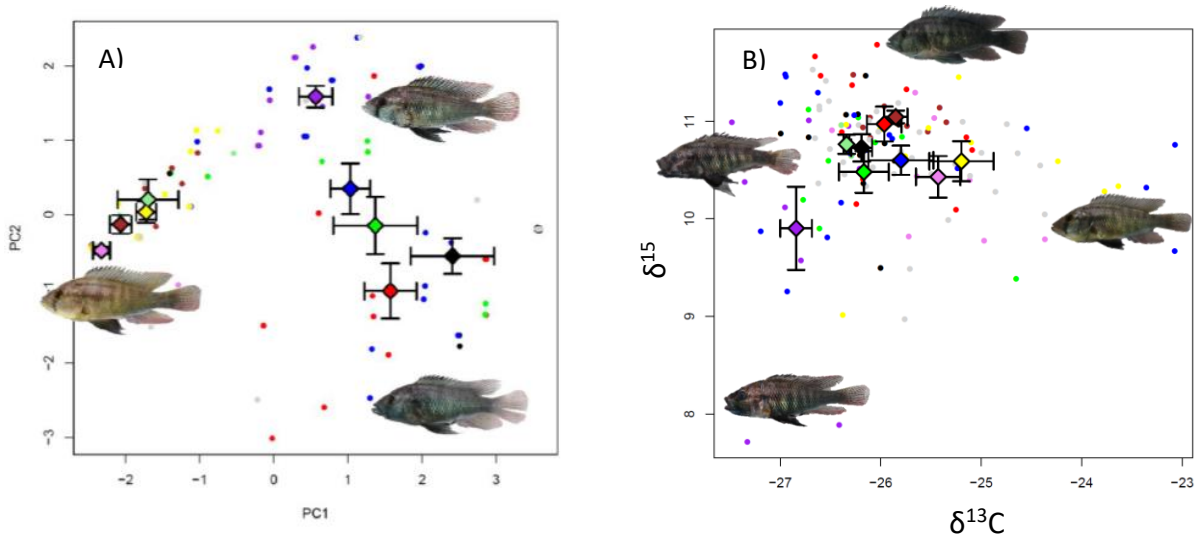


Figure S10: A) Variation and differentiation in male nuptial colouration (N=127) revealed three colour clusters with several morphs only occurring in one of those three groups (PLR, OSH, YBE, LEO in the most yellow/red cluster, PLB in the intermediate cluster, and LMO and GAL mainly in the blue/dark cluster). LEA and BBE occurred frequently in two of the three colour clusters. B) trophic variation and differentiation between the morphs of *Astatotilapia sp.* 'Chala' based on $\delta^{13}C$ and $\delta^{15}N$ stable isotopes, with pictures of the individual fish with the most extreme stable isotope ratios. The different colours of the symbols represent the different morphs, grey are individuals that could not be assigned to a morph. Dots represent individuals, whereas diamonds represent morph means with standard errors. Colours correspond to the colours assigned to the morphs throughout the manuscript.

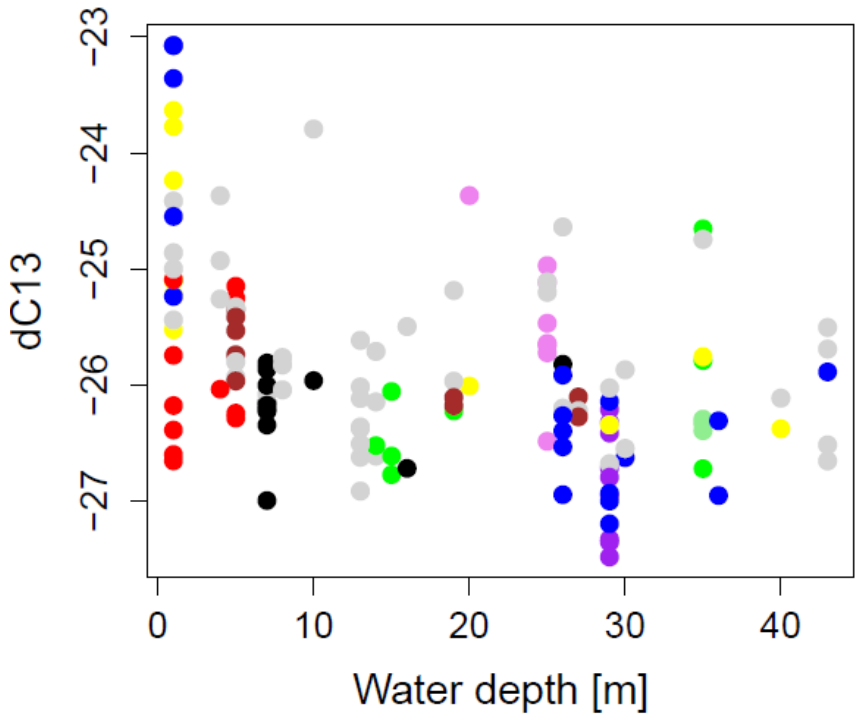


Figure S11: The $\delta^{13}C$ values for *Astatotilapia* in Lake Chala ranged from -27.5 to -23 and were strongly negative correlated with water depth, indicating that most fish were caught in the habitat where they lived and foraged (ANOVA: F = 3.17, df = 9, P = 0.001). The different colours of the dots represent the different morphs, grey dots are individuals that could not be assigned to a morph. Distinct differences between morphs within the same water depth are apparent in the shallow water but also in the depth range 25 to 30m. Colours correspond to the colours assigned to the morphs throughout the manuscript (blue = BBE, black = GAL, green = LEA, light green = LEO, brown = OSH, purple = PLB, violet = PLR, yellow = YBE).

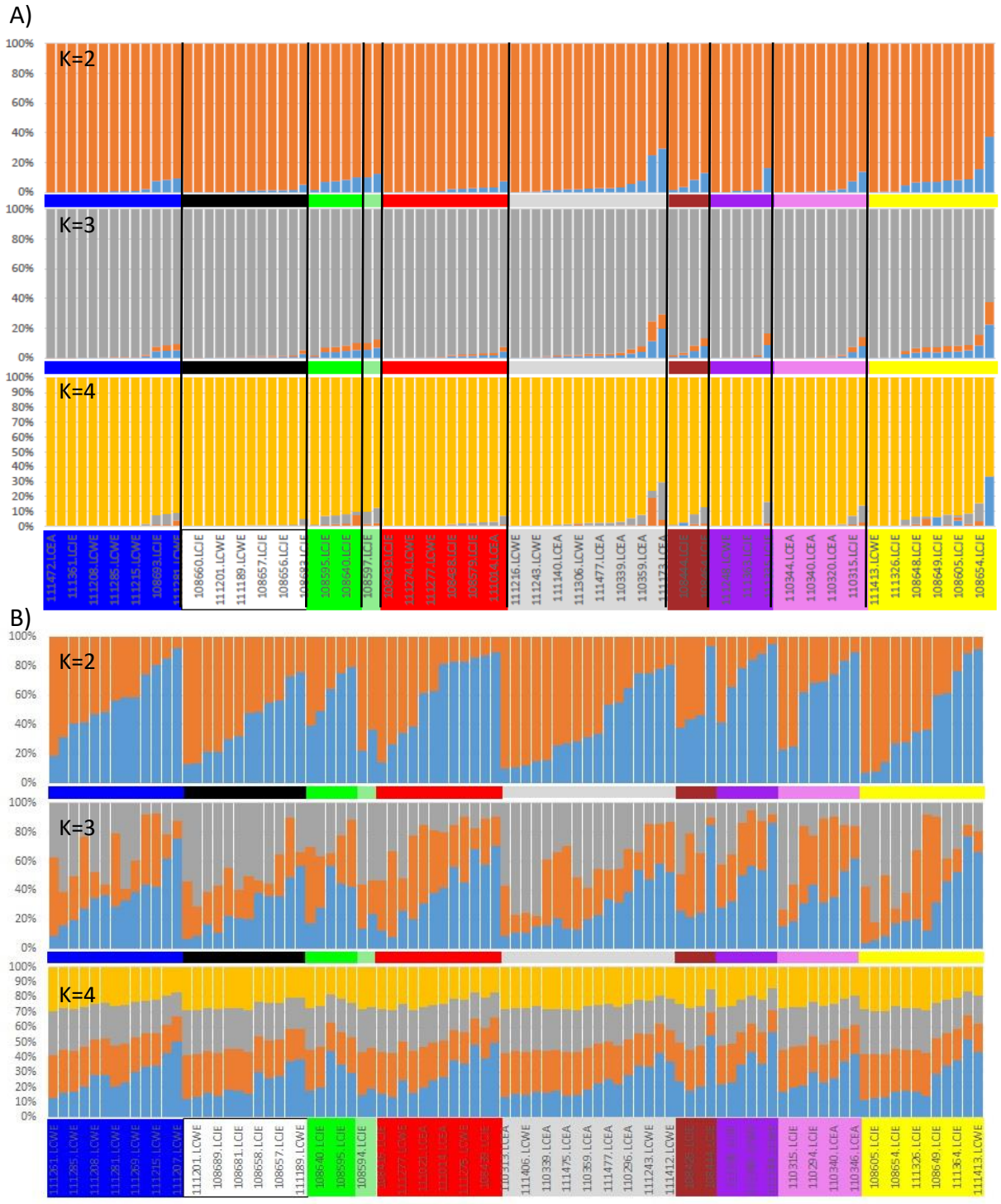
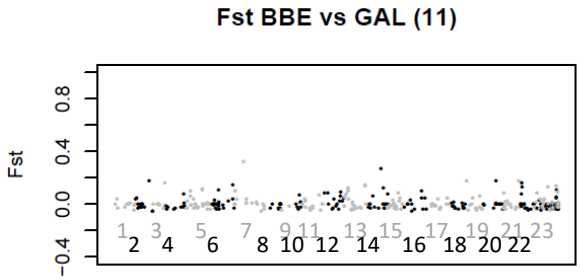
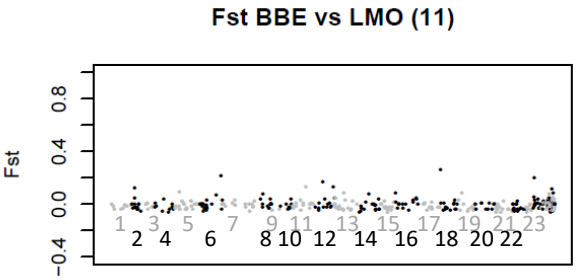
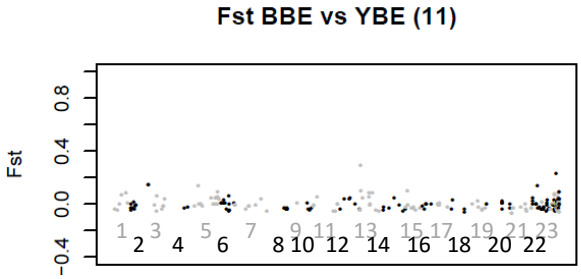
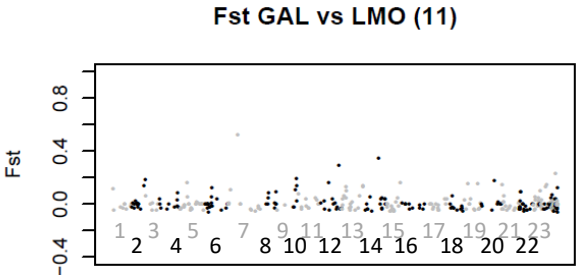


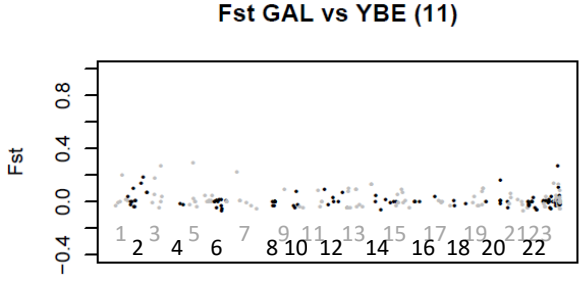
Figure S12: STRUCTURE-plots based on SNPs from RAD-sequencing for *Astatotilapia* from Lake Chala for K = 2 to K = 4 if aligned to the reference genome of *Oreochromis niloticus* (A) or *Metriaclima zebra* (B). Individuals are sorted by morph and then by assignment to the clusters detected in K = 2 for each A and B respectively. Colours bellow the STRUCTURE plots indicate the corresponding morphs (blue = BBE, black = GAL, green = LEA, light green = LEO, red = LMO, grey = unassigned, brown = OSH, purple = PLB, violet = PLR, yellow = YBE).

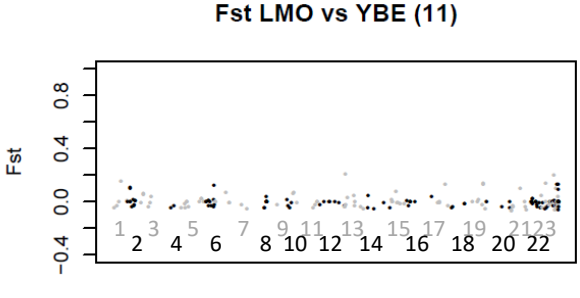

Fst BBE vs GAL (11)
Fst
−0.4 0.0 0.4 0.8
1 3 5 7 9 11 13 15 17 19 21 23
2 4 6 8 10 12 14 16 18 20 22

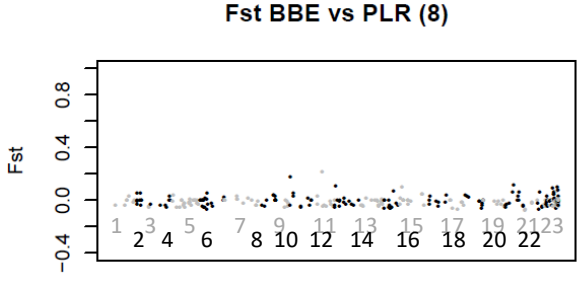

Fst BBE vs LMO (11)
Fst
−0.4 0.0 0.4 0.8
1 3 5 7 9 11 13 15 17 19 21 23
2 4 6 8 10 12 14 16 18 20 22

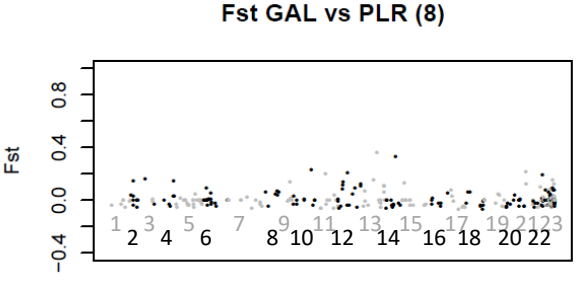

Fst BBE vs YBE (11)
Fst
−0.4 0.0 0.4 0.8
1 3 5 7 9 11 13 15 17 19 21 23
2 4 6 8 10 12 14 16 18 20 22

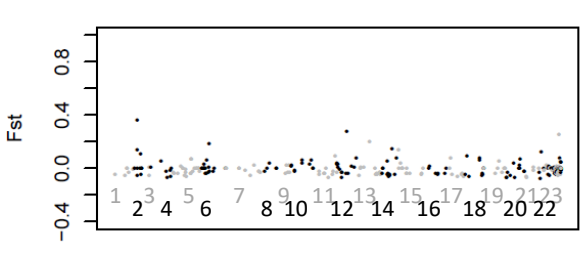

Fst GAL vs LMO (11)
Fst
−0.4 0.0 0.4 0.8
1 3 5 7 9 11 13 15 17 19 21 23
2 4 6 8 10 12 14 16 18 20 22

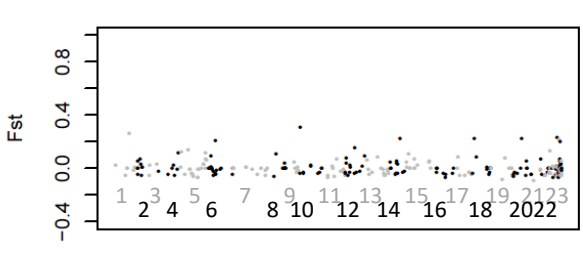

Fst GAL vs YBE (11)
Fst
−0.4 0.0 0.4 0.8
1 3 5 7 9 11 13 15 17 19 21 23
2 4 6 8 10 12 14 16 18 20 22

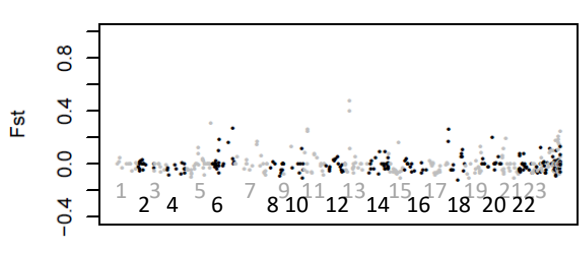

Fst LMO vs YBE (11)
Fst
−0.4 0.0 0.4 0.8
1 3 5 7 9 11 13 15 17 19 21 23
2 4 6 8 10 12 14 16 18 20 22

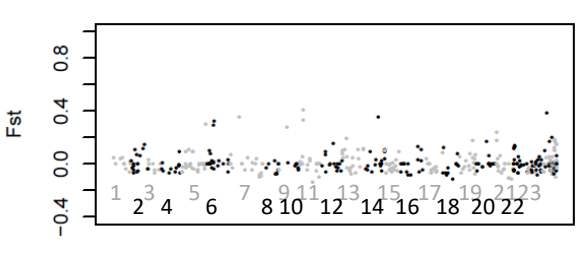

Fst BBE vs PLR (8)
Fst
−0.4 0.0 0.4 0.8
1 3 5 7 9 11 13 15 17 19 21 23
2 4 6 8 10 12 14 16 18 20 22

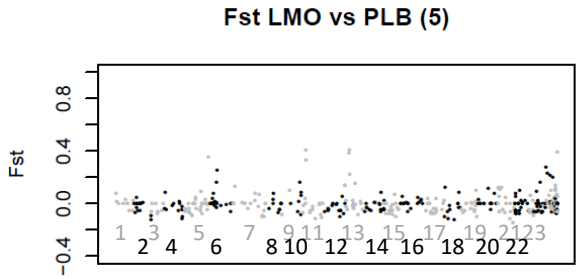

Fst GAL vs PLR (8)
Fst
−0.4 0.0 0.4 0.8
1 3 5 7 9 11 13 15 17 19 21 23
2 4 6 8 10 12 14 16 18 20 22

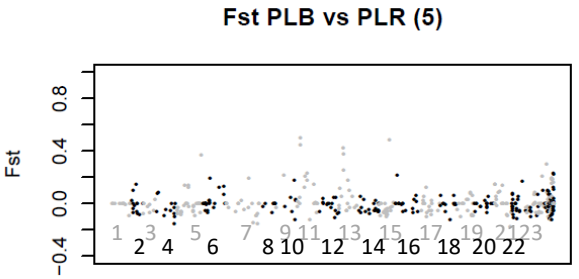

Fst LMO vs PLR (8)
Fst
−0.4 0.0 0.4 0.8
1 3 5 7 9 11 13 15 17 19 21 23
2 4 6 8 10 12 14 16 18 20 22

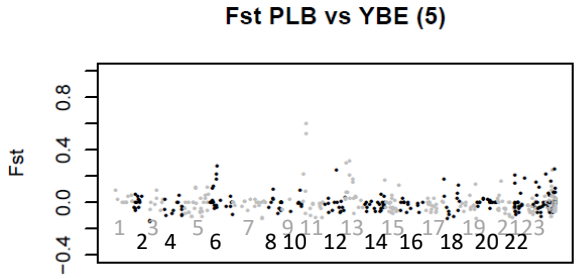

Fst PLR vs YBE (8)
Fst
−0.4 0.0 0.4 0.8
1 3 5 7 9 11 13 15 17 19 21 23
2 4 6 8 10 12 14 16 18 2022

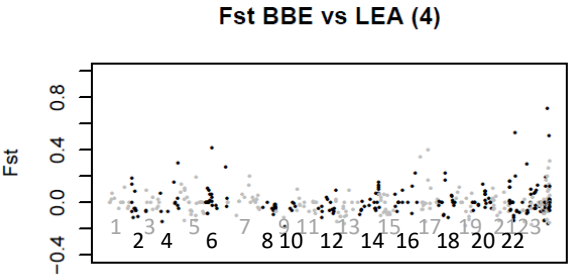

Fst BBE vs PLB (5)
Fst
−0.4 0.0 0.4 0.8
1 3 5 7 9 11 13 15 17 19 21 23
2 4 6 8 10 12 14 16 18 20 22

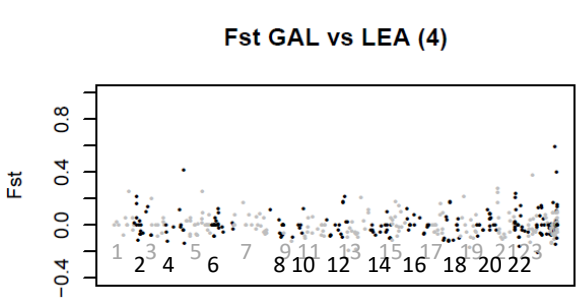

Fst GAL vs PLB (5)
Fst
−0.4 0.0 0.4 0.8
1 3 5 7 9 11 13 15 17 19 21 23
2 4 6 8 10 12 14 16 18 20 22

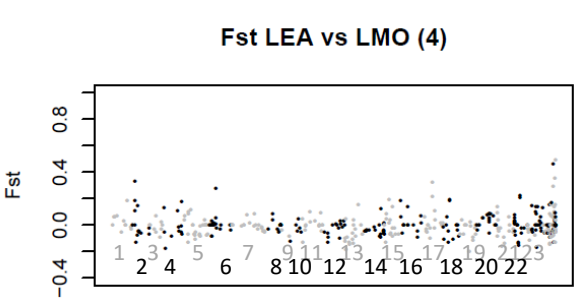

Fst LMO vs PLB (5)
Fst
−0.4 0.0 0.4 0.8
1 3 5 7 9 11 13 15 17 19 21 23
2 4 6 8 10 12 14 16 18 20 22

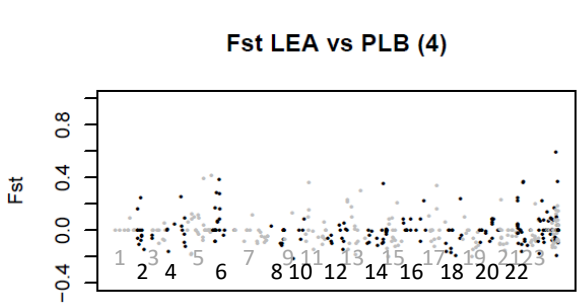

Fst PLB vs PLR (5)
Fst
−0.4 0.0 0.4 0.8
1 3 5 7 9 11 13 15 17 19 21 23
2 4 6 8 10 12 14 16 18 20 22

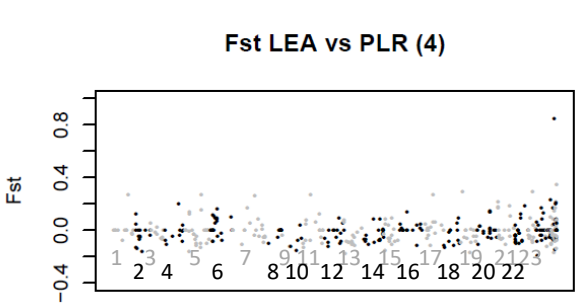

Fst PLB vs YBE (5)
Fst
−0.4 0.0 0.4 0.8
1 3 5 7 9 11 13 15 17 19 21 23
2 4 6 8 10 12 14 16 18 20 22

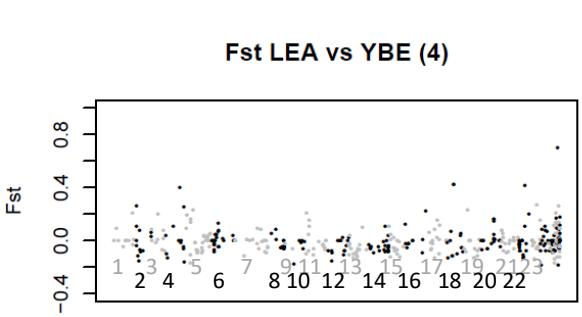

Fst BBE vs LEA (4)
Fst
−0.4 0.0 0.4 0.8
1 3 5 7 9 11 13 15 17 19 21 23
2 4 6 8 10 12 14 16 18 20 22

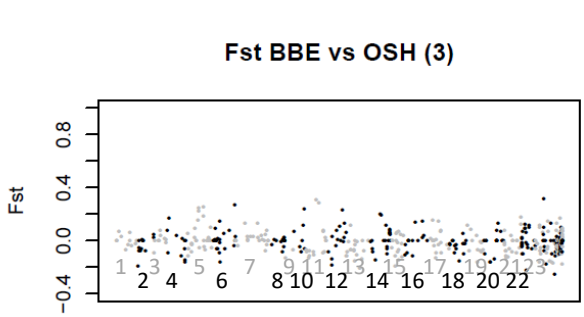

Fst GAL vs LEA (4)
Fst
−0.4 0.0 0.4 0.8
1 3 5 7 9 11 13 15 17 19 21 23
2 4 6 8 10 12 14 16 18 20 22

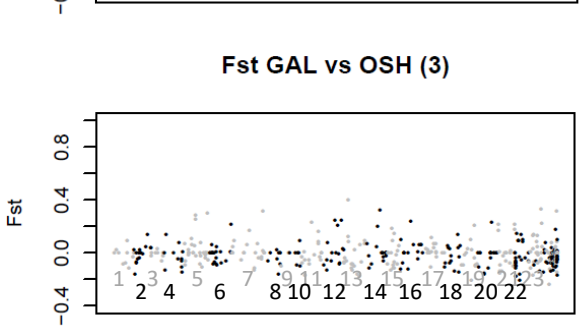

Fst LEA vs LMO (4)
Fst
−0.4 0.0 0.4 0.8
1 3 5 7 9 11 13 15 17 19 21 23
2 4 6 8 10 12 14 16 18 20 22

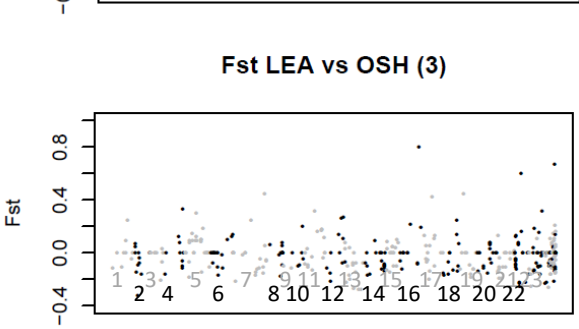

Fst LEA vs PLB (4)
Fst
−0.4 0.0 0.4 0.8
1 3 5 7 9 11 13 15 17 19 21 23
2 4 6 8 10 12 14 16 18 20 22


Fst LEA vs PLR (4)
Fst
−0.4 0.0 0.4 0.8
1 3 5 7 9 11 13 15 17 19 21 23
2 4 6 8 10 12 14 16 18 20 22


Fst LEA vs YBE (4)
Fst
−0.4 0.0 0.4 0.8
1 3 5 7 9 11 13 15 17 19 21 23
2 4 6 8 10 12 14 16 18 20 22


Fst BBE vs OSH (3)
Fst
−0.4 0.0 0.4 0.8
1 3 5 7 9 11 13 15 17 19 21 23
2 4 6 8 10 12 14 16 18 20 22


Fst GAL vs OSH (3)
Fst
−0.4 0.0 0.4 0.8
1 3 5 7 9 11 13 15 17 19 21 23
2 4 6 8 10 12 14 16 18 20 22


Fst LEA vs OSH (3)
Fst
−0.4 0.0 0.4 0.8
1 3 5 7 9 11 13 15 17 19 21 23
2 4 6 8 10 12 14 16 18 20 22

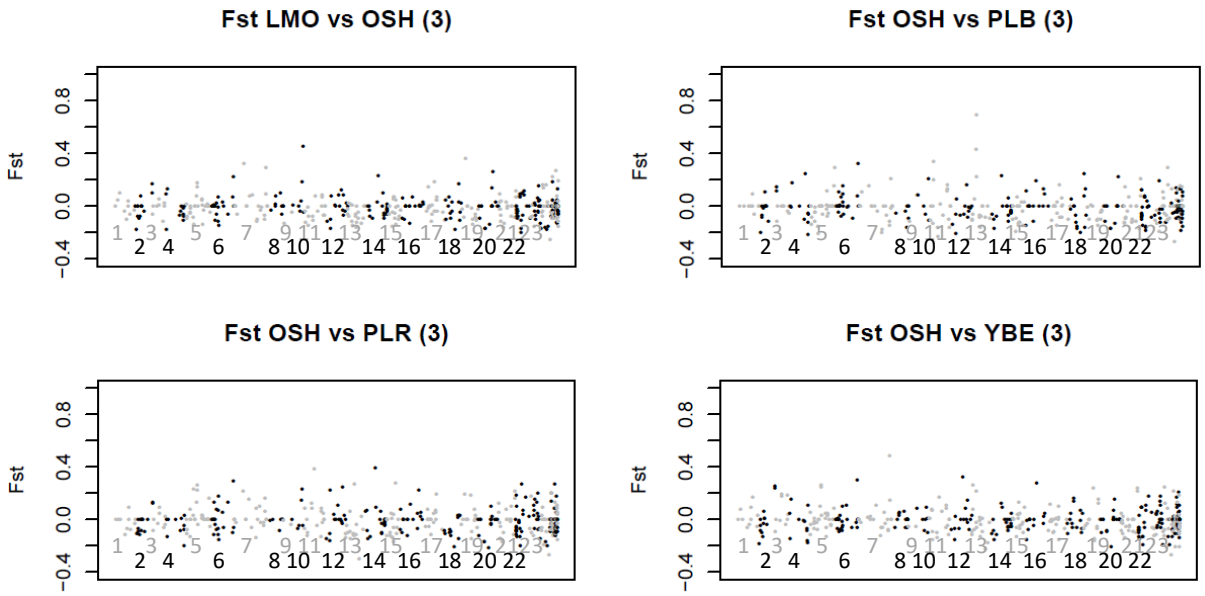


Figure S13: Manhattan-plots of genome scans for each pairwise comparison between morphs reveal that few SNPs distributed along the whole genome show increased differentiation between the different morphs within *Astatotilapia* sp. 'Chala'. To remove effects of uneven sample sizes between the morphs we subsampled 50 times for one genotype less than we had sequenced individuals in the morph with the smaller samples size (samples sizes per pairwise comparison are given in the brackets, for more details see appendix S2). Depicted on the y-axes is the average F_{ST} per SNP from the 50 subsamplings. Grey and black colours indicate the different linkage groups (labelled with roman numbers) in the reference genome of *Oreochromis niloticus* starting with LG1 in grey and subsequently all LG with uneven numbers in grey and the LG with even numbers in black.

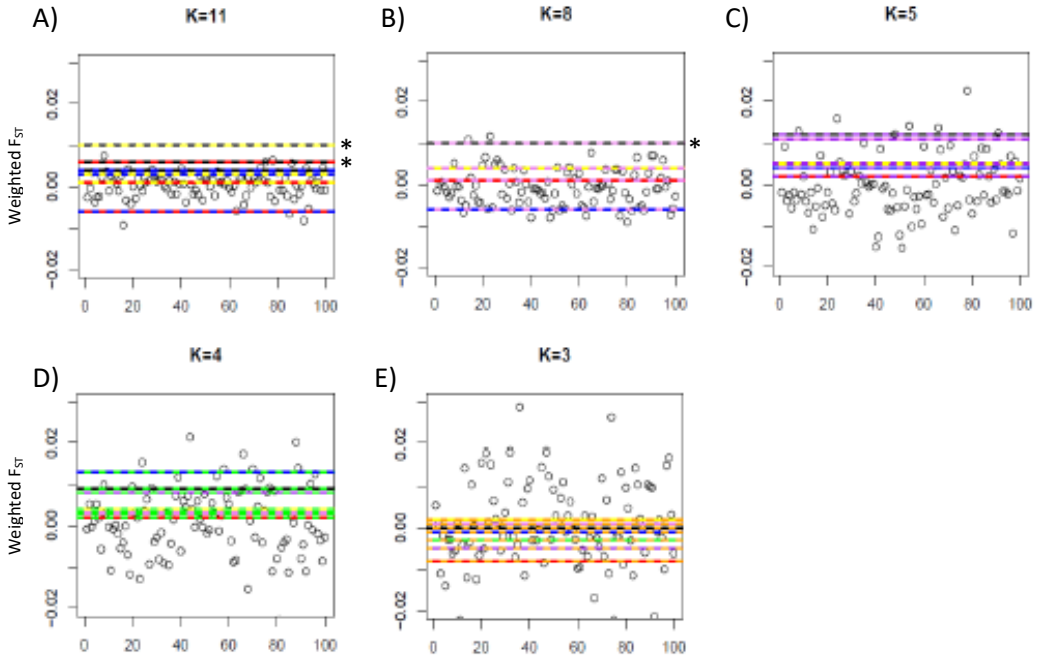


Figure S14: Permutation test to ask whether weighted pairwise F_{ST}s between morphs are higher than expected by chance given the genetic variation in the Lake Chala population. Dots and the y-axes represent the average weighted F_{ST} for 100 permutations, wherein we randomly subsampled the lake Chala population to two morphs of a sample size of K+1 and susbsampled each morph to K genotypes 50 times to calculate weighted F_{ST}s. The different panels represent the permutations for different Ks to match our observed data(K=11 (A), K=8 (B), K=5 (C), K=4 (D) and K=3 (E)). Lines represent the average weighted F_{ST} for the observed morph pairs with color indicating which morphs were part of each morph pair (blue = BBE, black = GAL, green = LEA, light green = LEO, red = LMO, brown = OSH, purple = PLB, violet = PLR, yellow = YBE, e.g. black/yellow line represents the morph pair GAL/YBE). Morph pairs with weighted F_{ST}s significantly higher than expected by chance (less than 5 of the 100 permutations with an F_{ST} higher than the observed value) are highlighted with an asterisk (panel A and B).

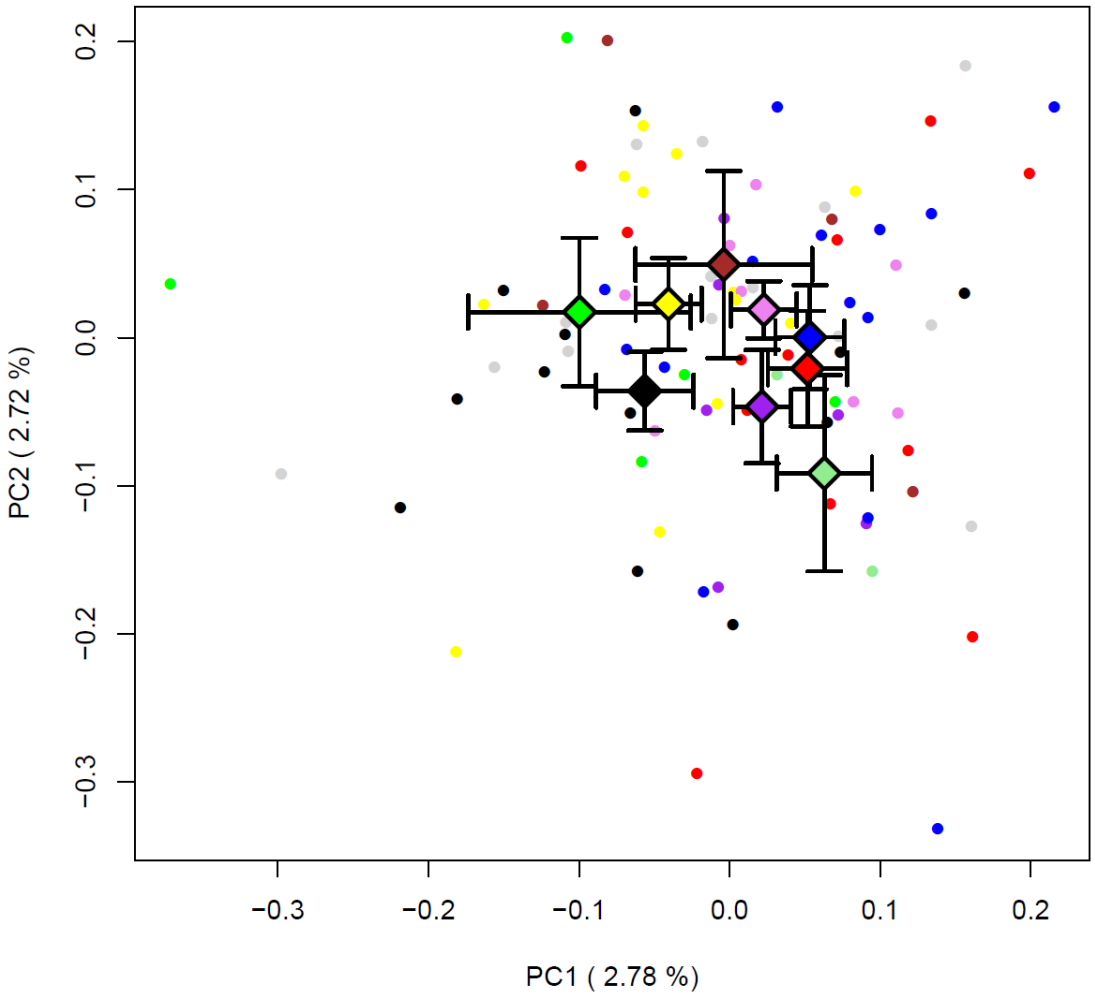
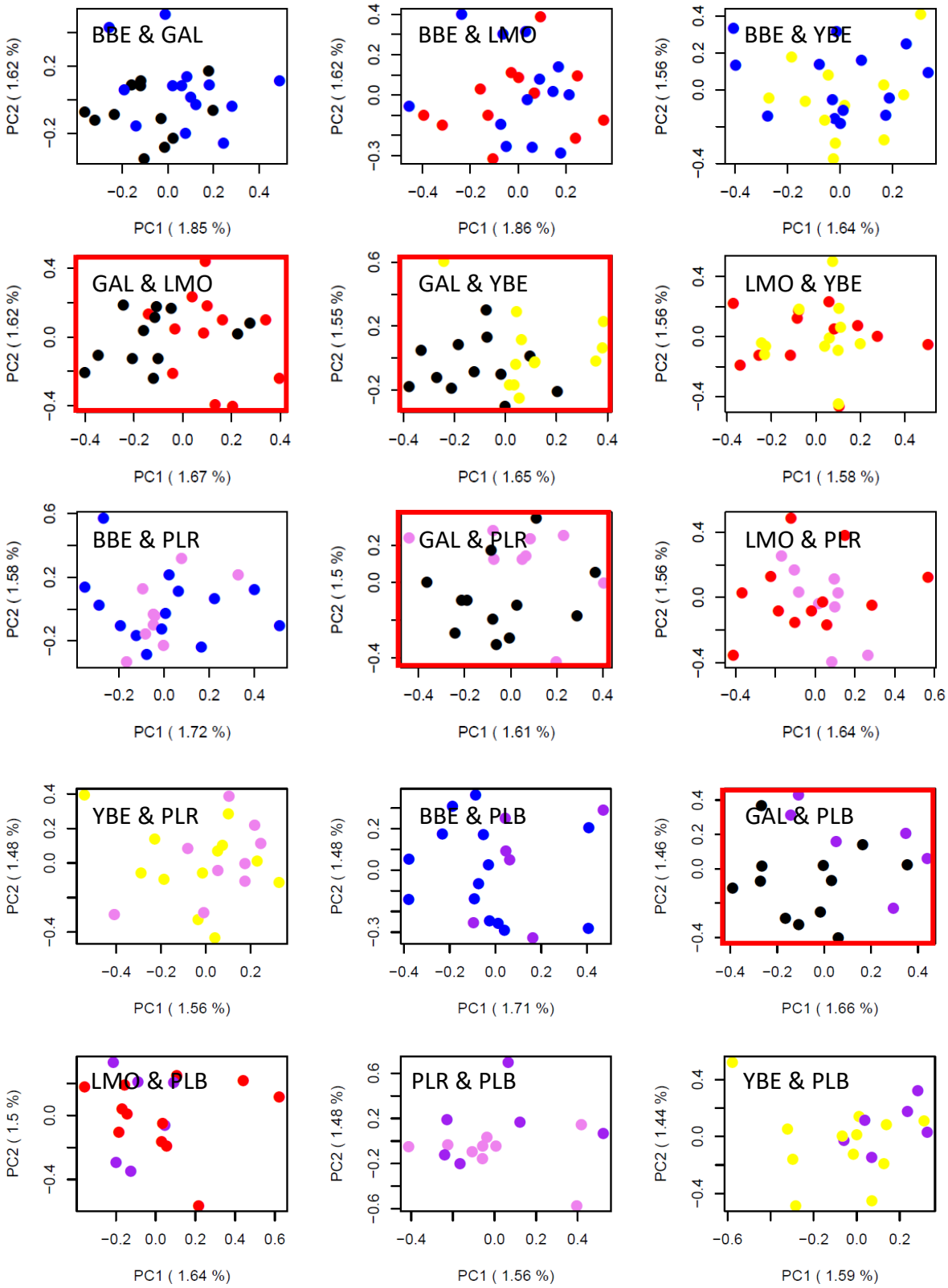


Figure S15: PCA-plot based on genomic RAD-sequencing data (aligned to *O. niloticus,* 514 SNPs retained for this plot). The different colours of the symbols represent the different morphs (see legend). Dots represent individuals, whereas diamonds represent morph centroids with standard errors (blue = BBE, black = GAL, green = LEA, light green = LEO, brown = OSH, purple = PLB, violet = PLR, yellow = YBE, light blue (in C) = Nyumba ya Mungu, grey = not assigned).


BBE & GAL
PC2 (1.62 %)
PC1 (1.85 %)
BBE & LMO
PC2 (1.62 %)
PC1 (1.86 %)
BBE & YBE
PC2 (1.56 %)
PC1 (1.64 %)
GAL & LMO
PC2 (1.62 %)
PC1 (1.67 %)
GAL & YBE
PC2 (1.55 %)
PC1 (1.65 %)
LMO & YBE
PC2 (1.56 %)
PC1 (1.58 %)
BBE & PLR
PC2 (1.58 %)
PC1 (1.72 %)
GAL & PLR
PC2 (1.5 %)
PC1 (1.61 %)
LMO & PLR
PC2 (1.56 %)
PC1 (1.64 %)
YBE & PLR
PC2 (1.48 %)
PC1 (1.56 %)
BBE & PLB
PC2 (1.48 %)
PC1 (1.71 %)
GAL & PLB
PC2 (1.46 %)
PC1 (1.66 %)
LMO & PLB
PC2 (1.5 %)
PC1 (1.64 %)
PLR & PLB
PC2 (1.48 %)
PC1 (1.56 %)
YBE & PLB
PC2 (1.44 %)
PC1 (1.59 %)

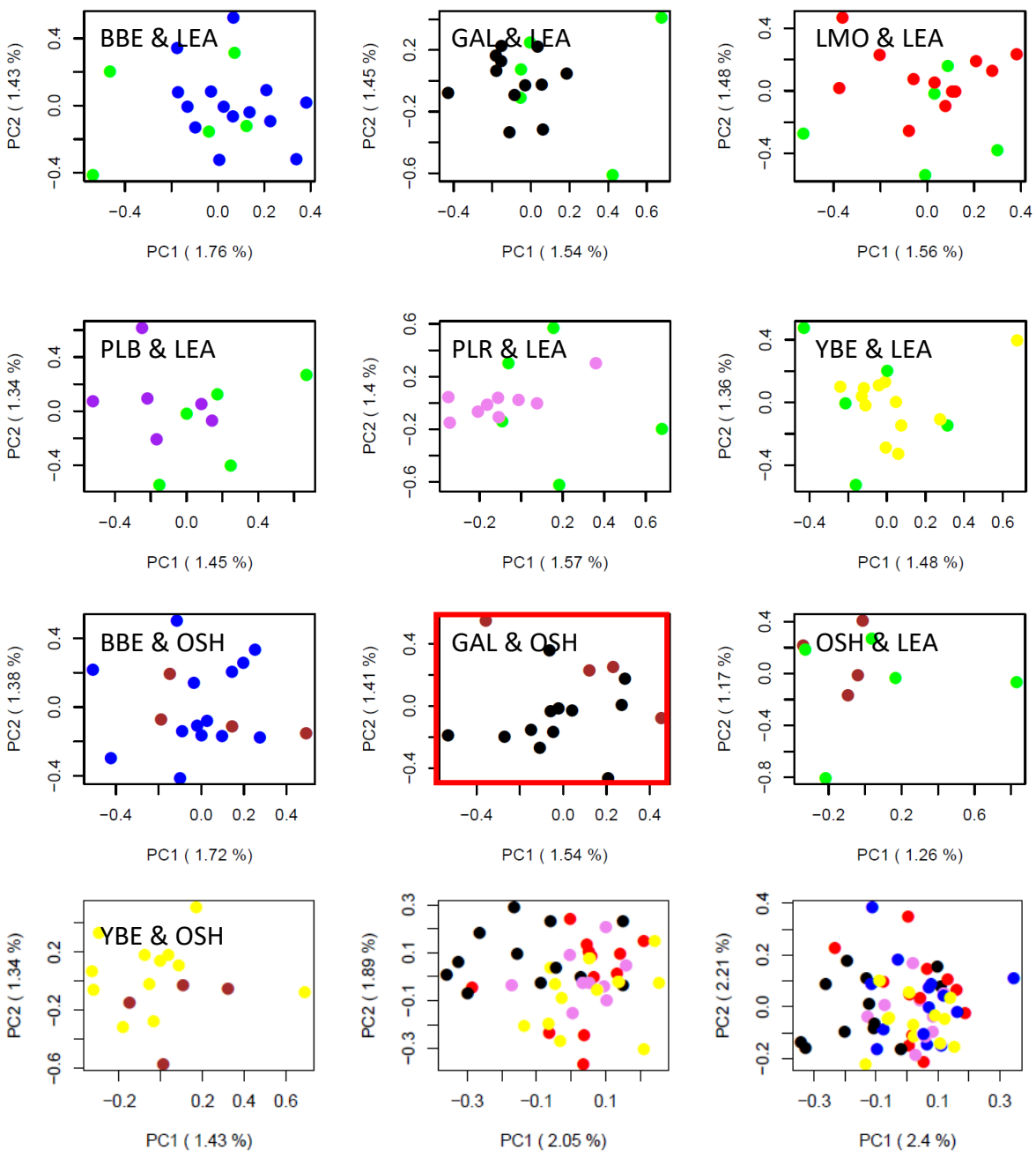


Figure S16: Genomic differentiation between morph pairs of *Astatotilapia* sp. 'Chala' in pairwise genomic PCA (aligned to *O. niloticus,* plots for the alignment to *M. zebra* are not shown). Whereas in most cases individuals do not cluster by morph, in some pairs they do, e.g. in GAL *vs* LMO, GAL *vs* YBE, GAL *vs* PLR, GAL *vs* PLB or GAL *vs* OSH (highlighted with red frames). The last two panels show all these four morphs that are part of genomic divergence in a shared PCA. They reveal that GAL seems to be the morph that drives the observed pattern, as it tends to cluster separately from all three other morphs. The panels are sorted to match the sequence in figure S15. Blue = BBE, black = GAL, green = LEA, light green = LEO, red = LMO, brown = OSH, purple = PLB, violet = PLR, yellow = YBE.

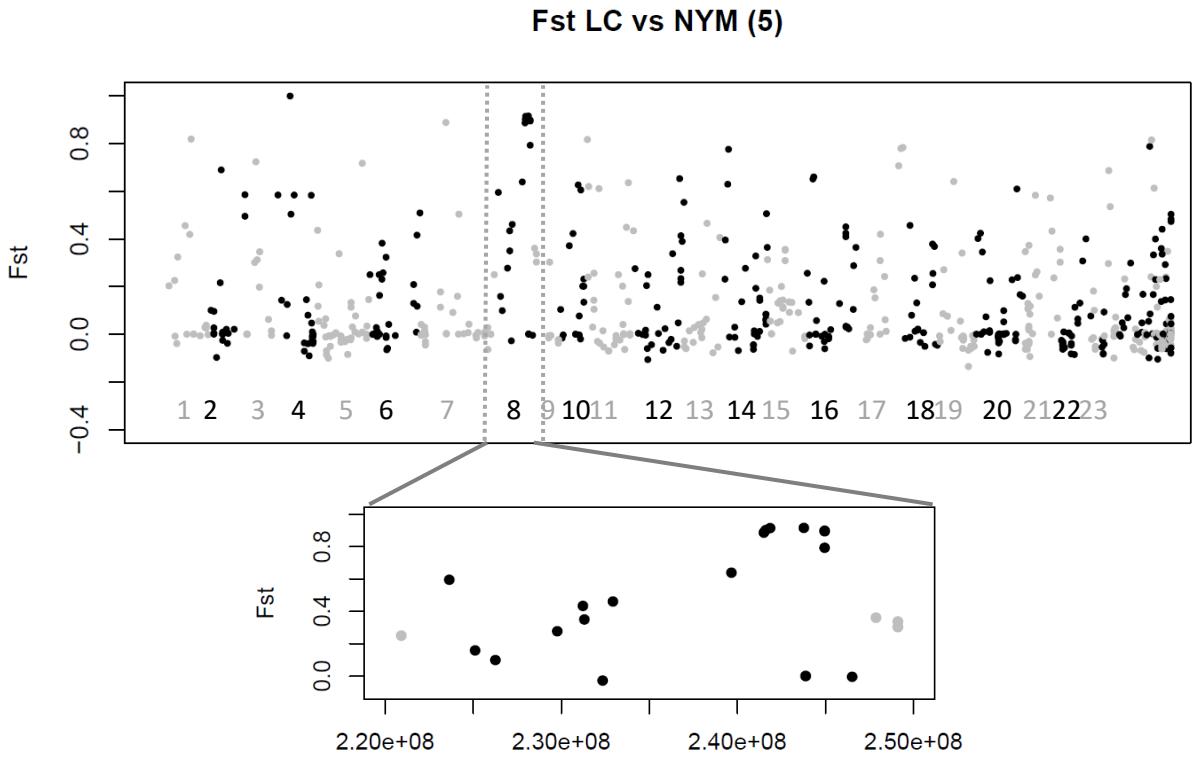


Figure S17: Manhattan-plot of the genome scan reveal that few SNPs distributed along the whole genome show increased differentiation between *Astatotilapia* of Lake Chala (LC) and *Astatotilapia cf. bloyeti* of the Nyumba ya Mungu (NYM) reservoir. The only region that might have an increased number of potentially subsequent highly differentiated SNPs is linkage groups 8. To account for different sample sizes between the two populations, we subsampled down to 5 genotypes per site per population 50 times. Depicted on the y-axes is the average F_{ST} per SNP from the 50 subsamplings. Grey and black colours indicate the different linkage groups with the corresponding number in the reference genome of *Oreochromis niloticus*. The labels on the x-axes of inset (LG8) indicates the position on the chromosome in base-pairs.

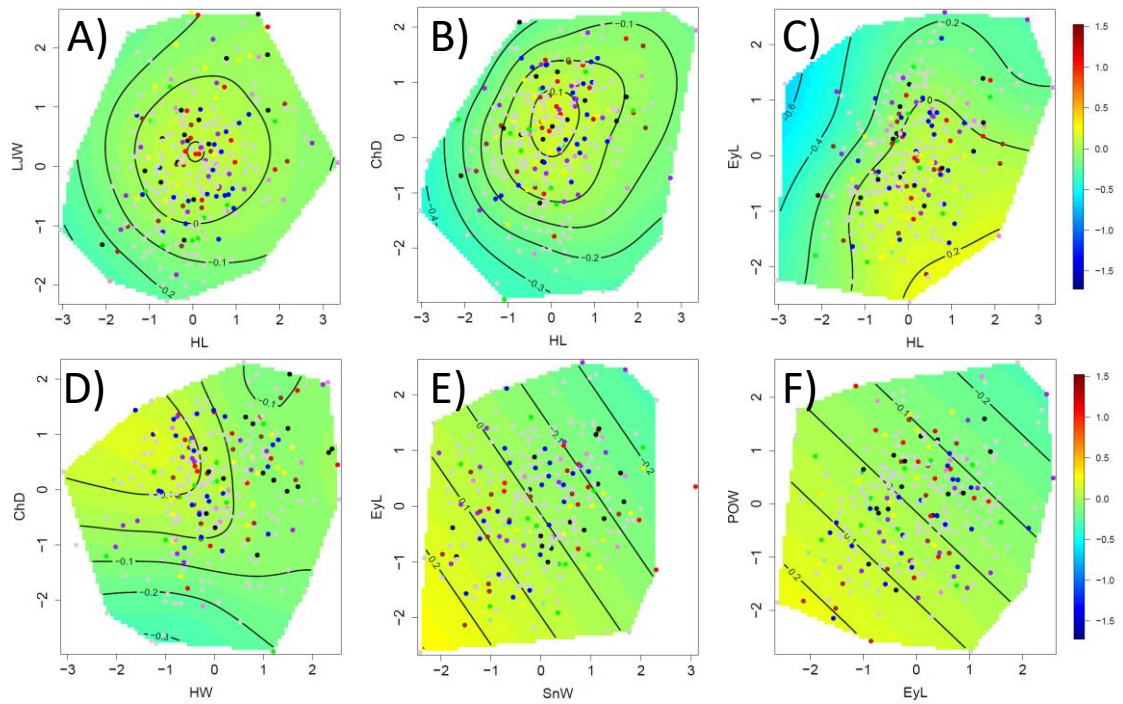


Figure S18: Fitness surfaces for the bivariate trait combinations that show significant correlational selection. A-D show stabilizing correlational selection, whereas E+F show directional correlational selection. The dots represent individuals, the colour of the dots corresponds to the different morphs. The background colour indicates estimated fitness, with high fitness indicated in warmer and low fitness in colder colours.

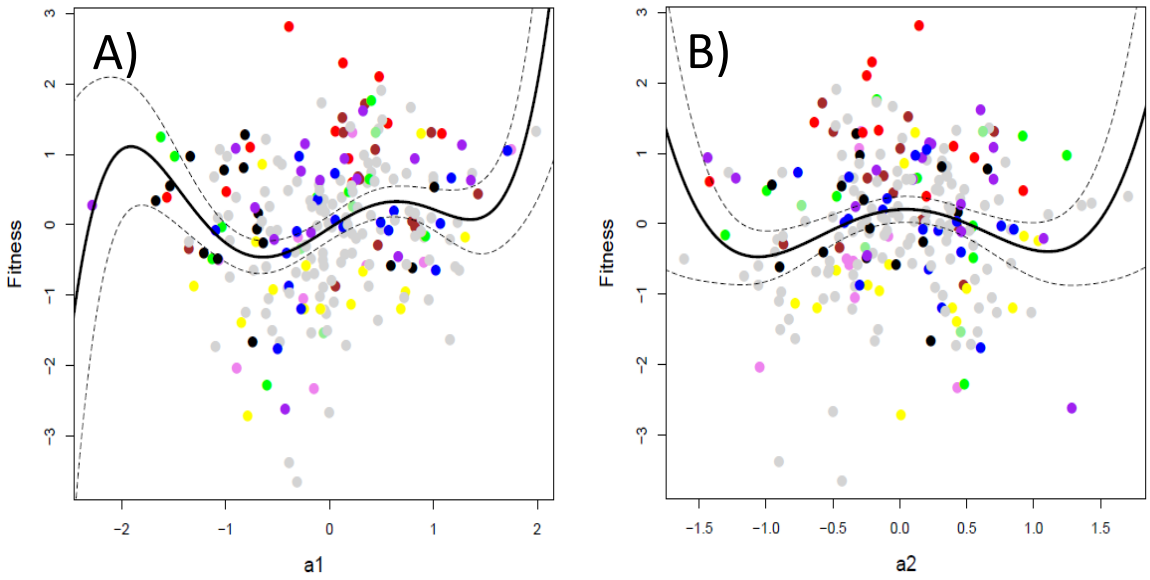


Figure S19: Relationship between A) a1 and B) a2 from the projection pursuit regression analyses on morphological traits, and the raw growth rate estimates. The pattern along a1 suggests evidence for two fitness peaks (around a1 = -1.9 and a1 = 0.7), whereas the main pattern along a2 suggests evidence for one fitness peak at a2 = 0.1. The colour of the dots represents the different morphs(blue = BBE, black = GAL, green = LEA, light green = LEO, red = LMO, grey = unassigned, brown = OSH, purple = PLB, violet = PLR, yellow = YBE).

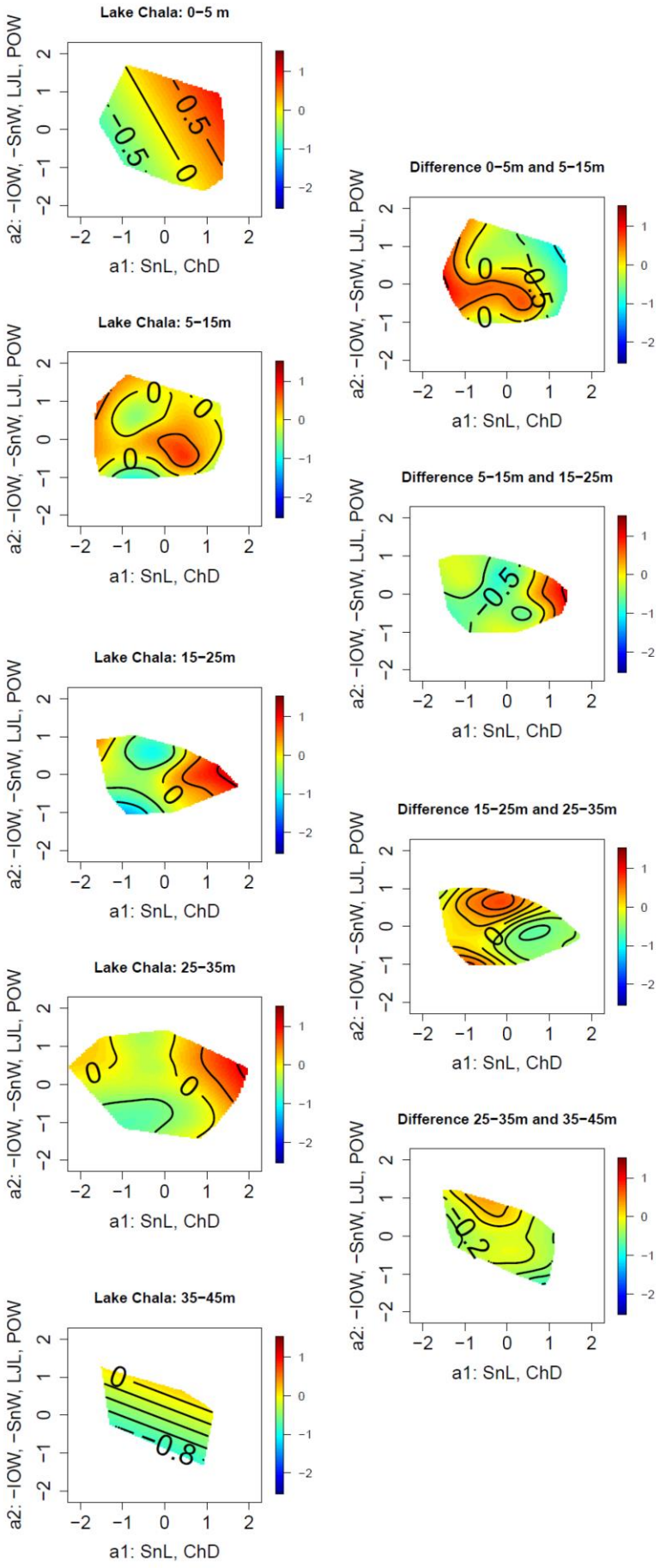


Figure S20: Change of the selection pattern along the depth gradient on the same morphological trait combination. On the left side, the fitness surfaces for the different depth categories are shown (identical to the ones in figure 3B). Surface colours represent smoothed estimated fitness values from red = high fitness to blue = low fitness. On the right side, we show the estimated fitness changes from the shallower to the deeper depth category. Surface colours represent smoothed fitness changes from one to the next fitness category from red = increase in fitness to blue = reduced fitness. Between 0-5m and 5-15m an additional fitness optimum for negative a1 emerges, while the optima at positive a1-values are reduced. Additionally, the two optima get connected at slightly negative a2. Between 5-15m the optimum at positive a1 moves slightly towards more positive a1, and gets higher, whereas the optimum at negative a1 moves slightly towards positive a2. The valley in between these two optima gets deeper by more than 0.5. Between 15-25m and 25-35m the surface becomes flatter, as the change mirrors the surface at 15-25m (optima get smaller, valleys less deep). And gets even flatter towards 35-45m.

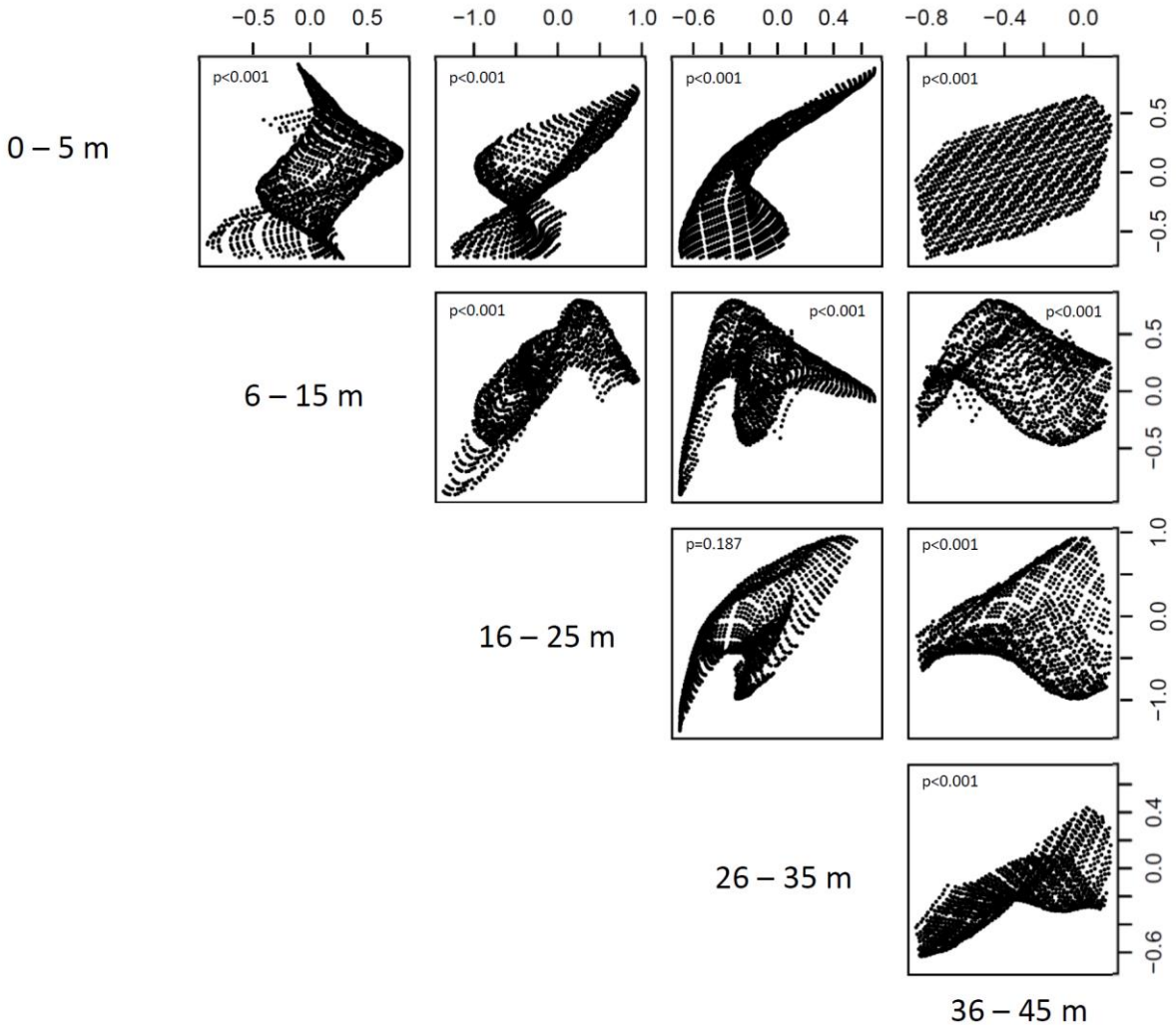


Figure S21: Pairwise comparison between the different fitness surfaces. Each plot shows the pairwise comparisons of the estimated fitness values for every grid in morphospace. Each dot represents the estimated fitness for the same grid in morphospace at two different water depths (one estimated fitness value as the x-coordinate and the other estimated fitness value as the y-coordinate). In the upper row, y-axes always represents the estimated fitness in the most shallow depth category (0 – 5m), the second row of the next depth category (6 – 15m) and so forth. In the left-most column the x-axis represents the estimated fitness in the depth habitat between 6 and 15 m, in the second column that for the next deeper habitat (16 to 25m) and so forth. P-values indicate the results from the paired Wilcoxon signed rank test. All fitness surfaces are different, except the fitness surfaces at 16 – 25m and the fitness surface at 26 – 35m where we could not reject the null hypothesis of no difference.

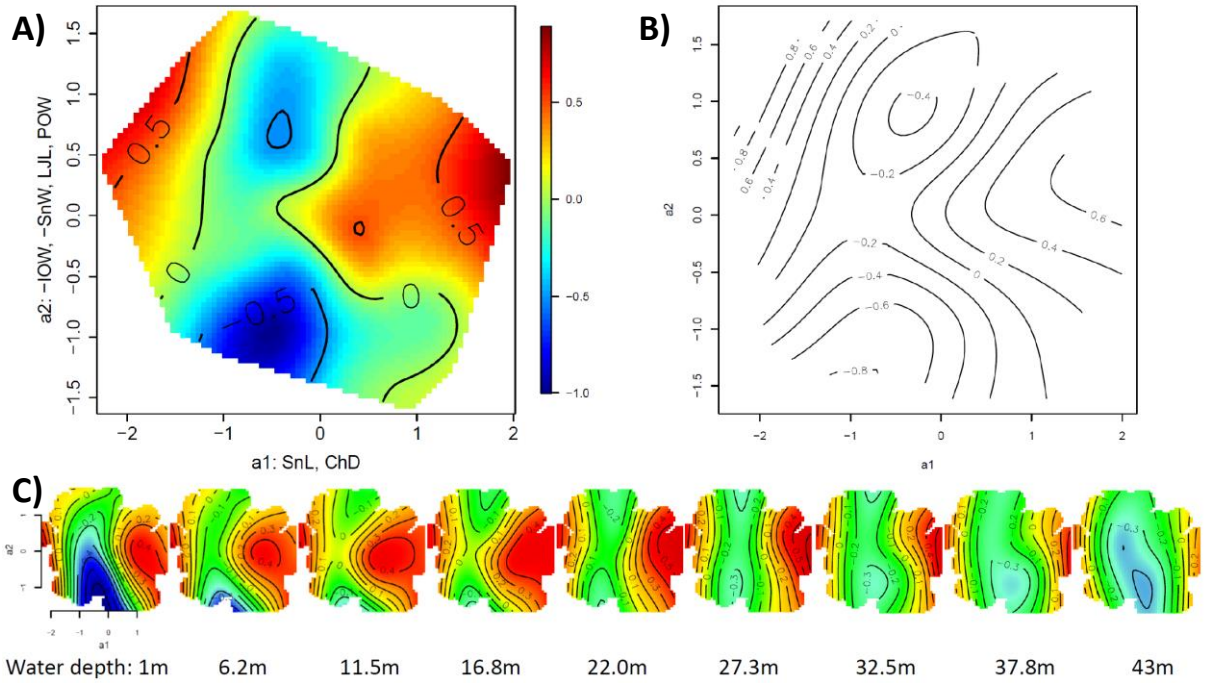


Figure S22: Graphic output of the generalized additive models (GAM). A) The original contour plot from the Projection Pursuit Regression analyses, B) the estimated surface based on GAM and with the raw growth measurements as the response variable and a1 and a2 with a tensor product interaction and a thin-plate spline smoothing parameter, and C) additionally including a tensor product interaction with water depth. The depth indicated with 11.5 is the only depth where the "bridge" between the two high-fitness areas (red) does remain above 0. In more shallow, as well as in deeper water, the valley is more severe. AIC-values were smaller for C) (645.5) than for B) (647.6) indicating a better fit if depth is taken into account.

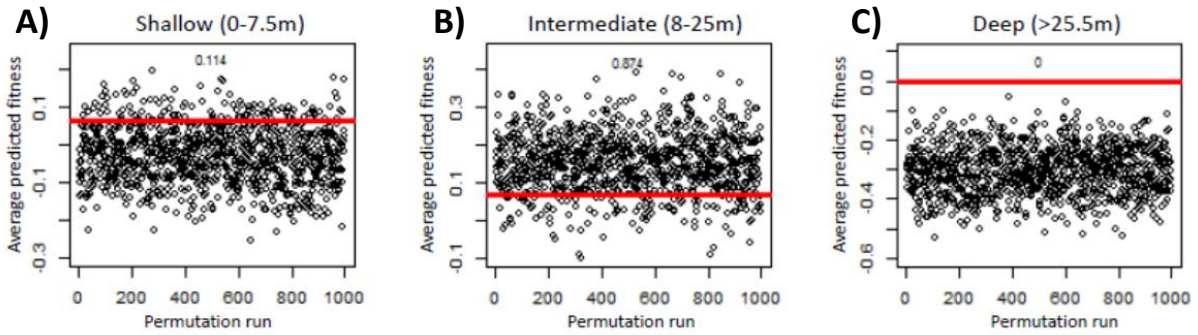


Figure S23: Predicted average fitness of the *Astatotilapia* in Lake Chala in a thousand permutations of randomly distributing individuals on the fitness surface for the three different depth categories. A) For the shallow water depth (0-7.5m), B) for the intermediate water depth (8-25m) and C) for the deep water depth (>25.5m). Each dot represents the predicted average fitness of one permutation. The red lines represent the actually observed predicted average fitness. The values on the plots indicate the fraction of permutations in which the predicted average fitness of all individuals if randomly distributed on the fitness surface exceeded the observed fitness prediction (similar to P-values). In the shallow and deep habitat more individuals are associated with areas of higher fitness than expected by chance (highly significant for the deep habitat), whereas this is not the case for the intermediate depth habitat.

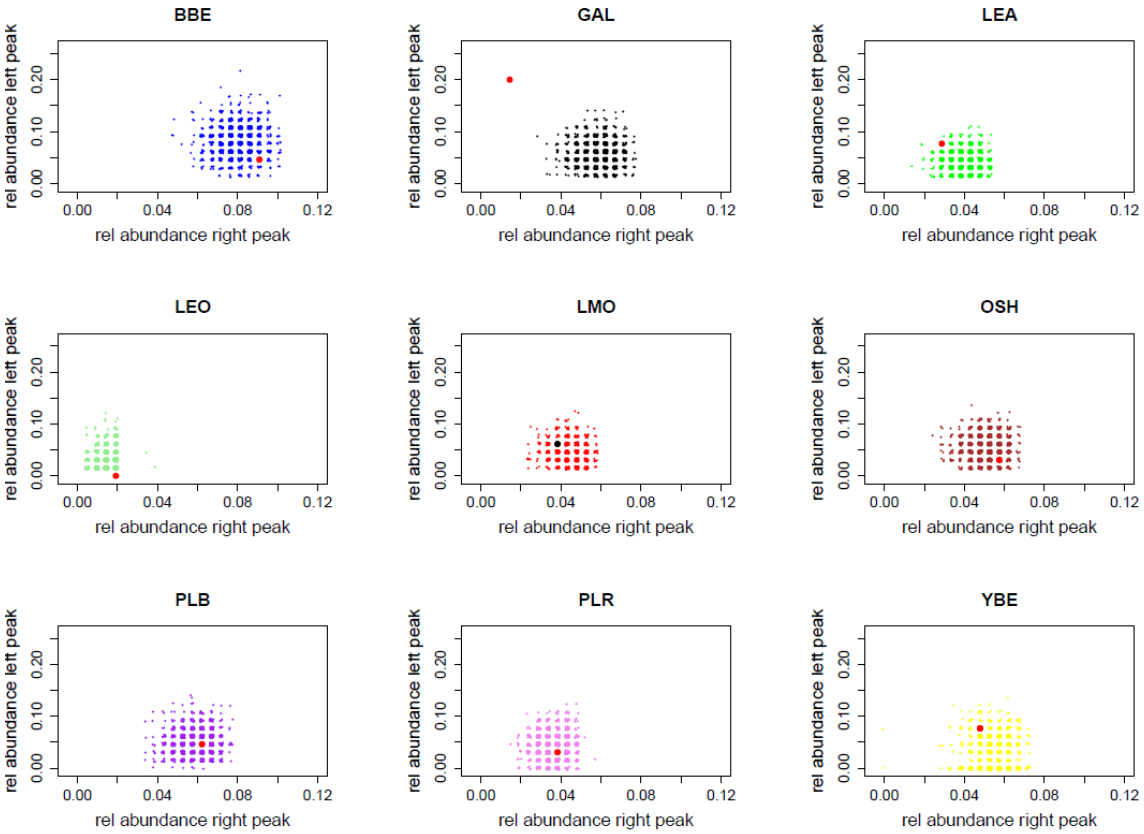
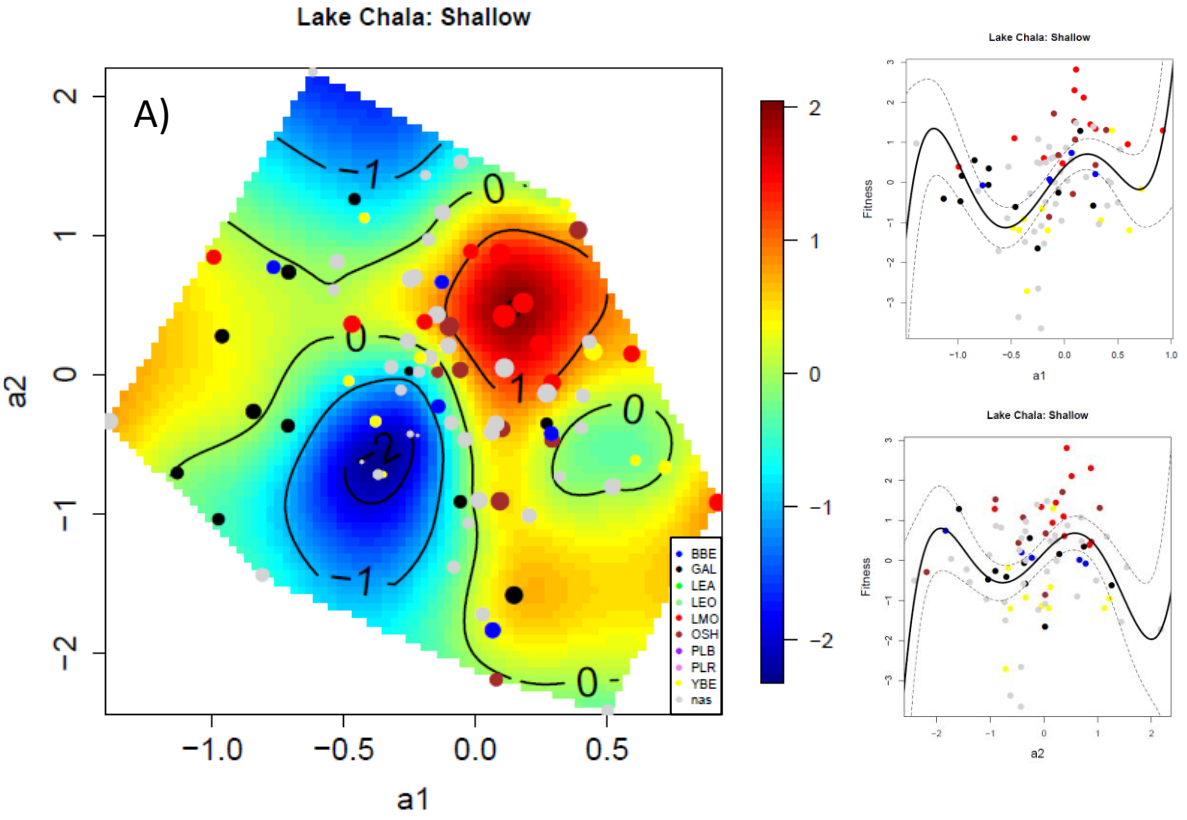
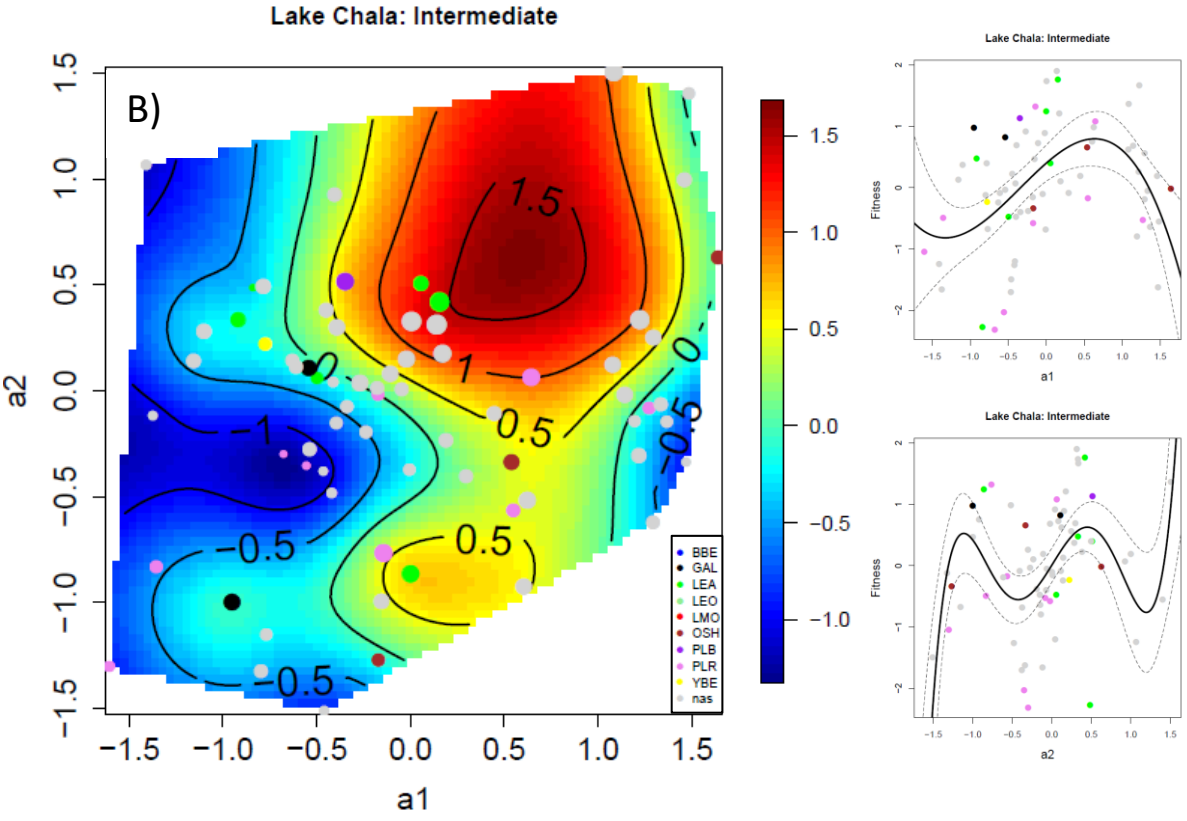


Figure S24: Predicted and observed relative abundances on the left and the right fitness peak based on 1000 permutations per morph for the fitness surface estimated over the entire range of water depths. The larger red dot (black in case of LMO) represents the observed value, the smaller dots in the colour of the different morphs matching the other figures, represent the expected values if the abundance of each morph on each peak would be similar as the abundance of each morph in the lake. GAL was significantly more abundant on the left peak ($P < 0.001$) and significantly less abundant on the right peak ($P < 0.001$) than expected by chance. LEA was significantly less abundant on the right peak ($P = 0.025$), whereas LEO was significantly less abundant on the left peak ($P < 0.001$) than expected by chance.


Lake Chala: Shallow
A)
a1
a2
BBE
GAL
LEA
LEO
LMO
OSH
PLB
PLR
YBE
nas
Fitness


Lake Chala: Intermediate
B)
a1
a2
BBE
GAL
LEA
LEO
LMO
OSH
PLB
PLR
YBE
nas
Fitness

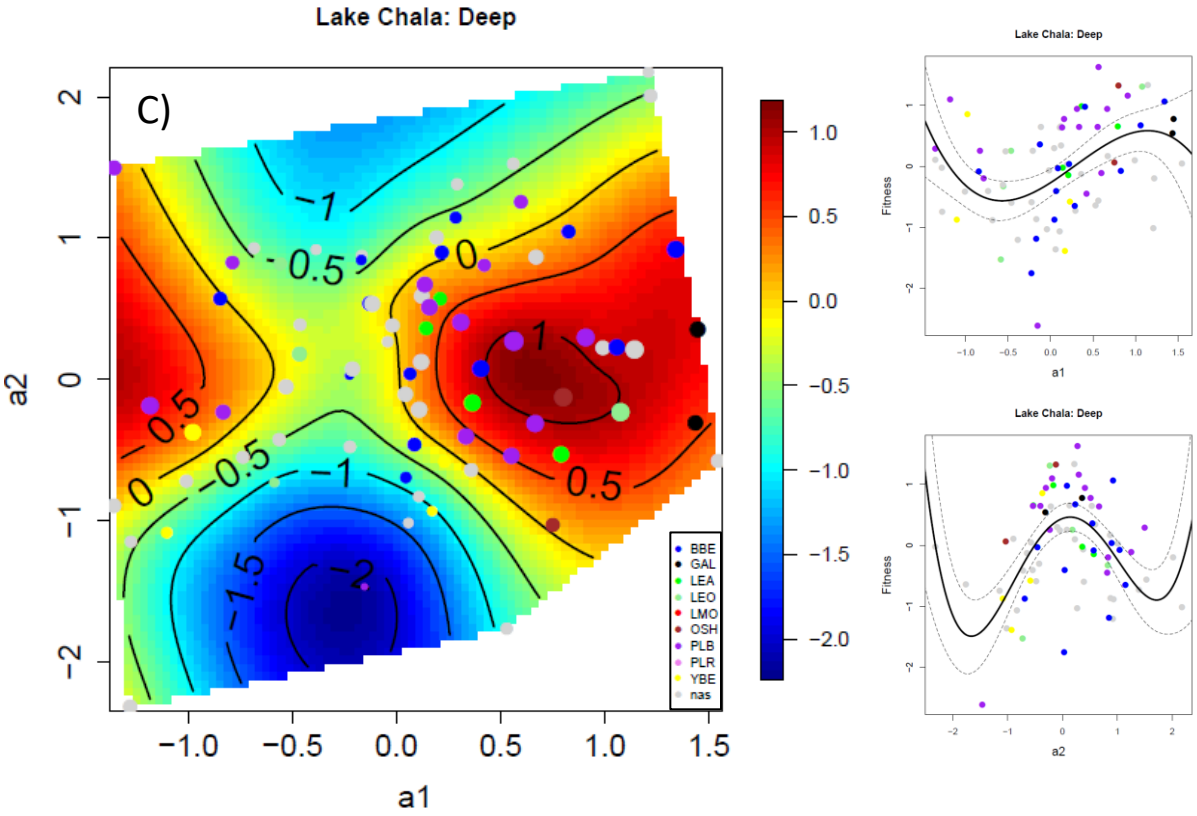


Figure S25: Fitness surfaces for *Astatotilapia sp*. 'Chala` based on Projection Pursuit Regression analysis (left side) and relationship between the two projections of the PPR analysis with the raw growth rate (right side) for the three different depth categories. The axes in the three panels are different because every projection (a1 and a2) has been calculated for each depth category separately. Evidence for two distinct fitness peaks was found on a1 (SnL, -SnW, POW, -HL) in the shallow water habitat (from the surface to 7.5m of depth (A)), on a2 (SnW, -EyD,-POW) in the intermediate depth habitat (B: 8 - 25 m water depth) and on a1 (HL, -PPL, -BD, -EyD) in the deep habitat (C: 25.5 - 47 m water depth). The colour of the dots corresponds to the different morphs, grey are individuals that could not be assigned to a morph. The background colour show areas of estimated fitness, with high fitness indicated in red and low fitness indicated in blue.

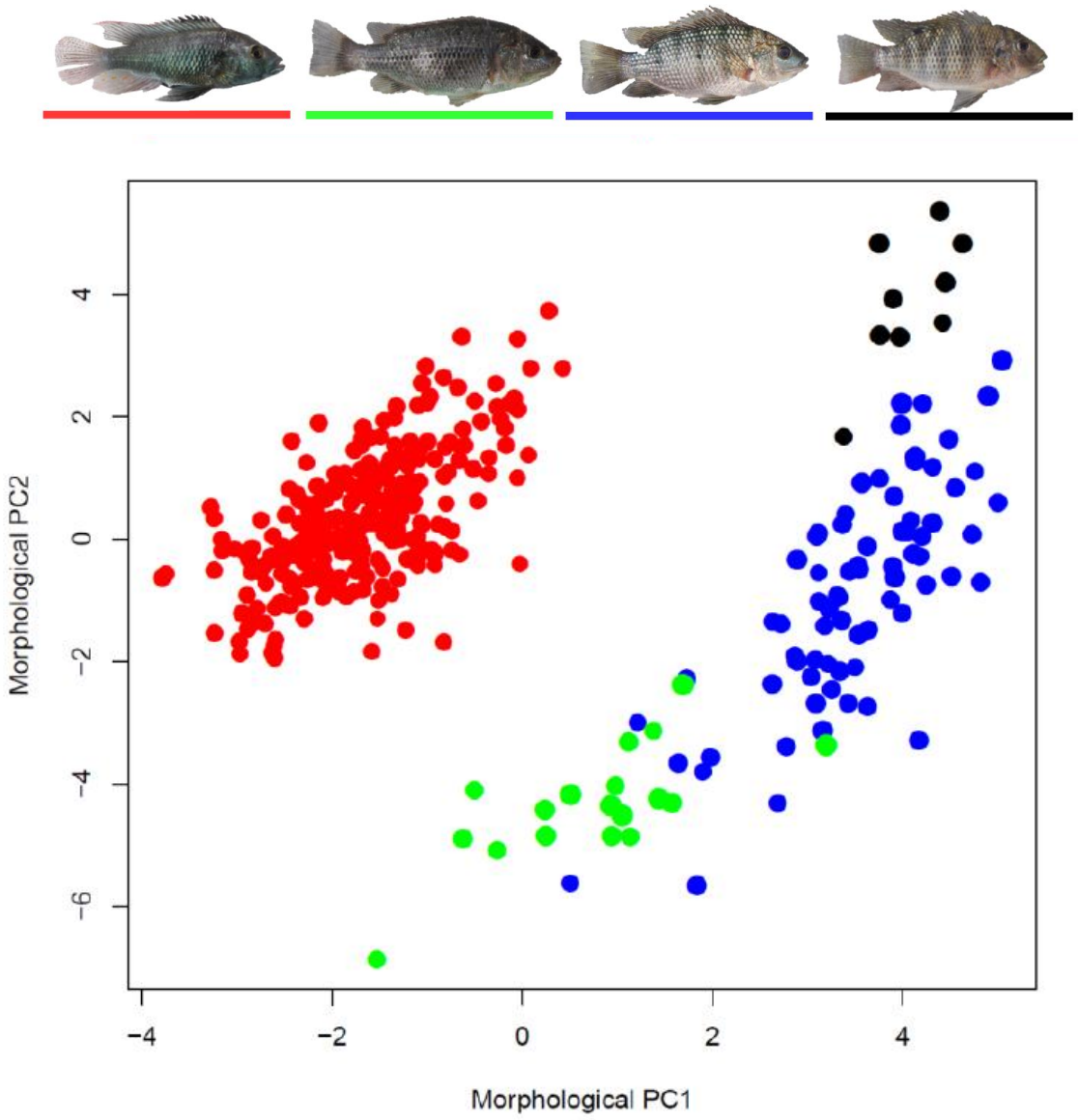


Figure S26: Morphological variation in the fish community of Lake Chala represented by a PC-plot on linear morphological traits of the four fish species that occur in Lake Chala: *Astatotilapia* sp. 'Chala' (red), the endemic *Oreochromis hunteri* (green), *O.* sp. 'blue head' (blue) and *Coptodon rendalli* (black). Morphologically, *Astatotilapia* does not overlap with either of the others. There is similarly little overlap in stable isotopic signatures of diet (24). Both types of data indicate that *Astatotilapia* may not experience much interspecific competition in Lake Chala.

Table S1: Sample sizes of *Astatotilapia* for the different analyses. The analyses vary in sample size for various reasons. For instance, colour analyses were restricted to individuals that still expressed nuptial coloration upon taking the life pictures, and sample size for stomach contents is low, because we focussed on the individuals we could assign to morphs and that had a stomach that is at least 25% full.

N per analysis	Total	BBE	GAL	LEA	LEO	LMO	OSH	PLB	PLR	YBE	nas	NYM
Morphology	284	22	16	11	4	12	14	16	10	15	154	10
Colour	84	18	7	2	2	12	8	1	4	15	15	0
Stomach content	67	13	7	5	0	8	10	5	3	10	0	6
Stable isotopes	133	18	12	8	3	11	9	9	8	10	45	0
Scales	231	18	15	10	4	11	13	16	9	15	120	0
Mt haplotype	78	14	8	6	1	12	5	4	9	10	5	4
RAD sequencing	96	15	12	5	2	12	4	6	9	12	13	6

Table S2: ID, morph-assignment, site of capture, capture depth (in meter), the number of raw reads and the mean sequencing depth of the 90 samples from *Astatotilapia sp*. 'Chala' used for RAD sequencing. JE is located at the north-western tip of the lake, EA at the boarder to Kenya on the eastern side of the lake and WE at the boarder to Kenya on the western side of the lake. Nas indicate individuals that could not be assigned to either morph due to the bad shape of the fish (due to net-predation of the endemic crabs) or due to the loss of colouration after capture.

ID	Morph	Site	Capture Depth	# raw reads	Mean depth	ID	Morph	Site	Capture Depth	# raw reads	Mean depth
108416	LMO	JE	5	2210821	43.49	110350	YBE	EA	20	919654	14.38
108426	OSH	JE	5	1807194	32.07	110352	PLR	EA	25	2336538	43.63
108438	LMO	JE	5	2607945	49.05	110359	nas	EA	10	1069822	20.45
108439	LMO	JE	5	5795523	105.85	111008	LMO	EA	1	1225156	19.61
108440	LMO	JE	5	3359650	61.23	111014	LMO	EA	1	1569425	25.83
108444	OSH	JE	5	1274489	26.58	111021	LMO	EA	1	2048282	37.07
108446	OSH	JE	5	2623460	48.26	111140	nas	EA	30	1274348	19.09
108464	OSH	JE	27	1640104	33.42	111173	nas	EA	35	756903	12.97
108579	LMO	JE	4	2790976	50.59	111177	YBE	EA	35	2368057	38.52
108594	LEO	JE	35	642887	10.54	111189	GAL	WE	10	1915293	32.97
108595	LEA	JE	35	1594372	28.46	111200	GAL	WE	26	1336772	22.27
108597	LEO	JE	35	1031664	22.58	111201	GAL	WE	26	1919000	33.37
108600	LEA	JE	35	944410	20.81	111207	BBE	WE	26	2542819	40.93
108605	YBE	JE	35	641470	15.96	111208	BBE	WE	26	2083008	37.78
108606	LEA	JE	35	1282350	24.45	111215	BBE	WE	26	2813450	42.20
108640	LEA	JE	15	1506759	27.07	111216	nas	WE	26	2802756	48.02
108645	LEA	JE	15	2369817	48.55	111228	PLB	WE	29	1508002	25.51
108648	YBE	JE	1	1017897	21.24	111240	PLB	WE	29	4478864	74.19
108649	YBE	JE	1	913244	20.55	111243	nas	WE	29	2081524	38.52
108650	YBE	JE	1	929953	18.74	111244	PLB	WE	29	2539838	49.03
108654	YBE	JE	1	1170450	21.17	111248	PLB	WE	29	2626962	43.15
108656	GAL	JE	7	1681678	29.77	111261	BBE	WE	29	2744946	44.01
108658	GAL	JE	7	2094125	33.39	111269	BBE	WE	36	1381555	24.91
108660	GAL	JE	7	4543520	49.35	111270	nas	WE	36	959895	16.47
108680	GAL	JE	7	2132198	30.05	111274	LMO	WE	1	3388986	55.33
108681	GAL	JE	7	2232937	35.33	111275	LMO	WE	1	2894794	47.41
108683	GAL	JE	7	2204154	44.70	111277	LMO	WE	1	4597091	72.76
108685	GAL	JE	7	2614040	51.31	111280	LMO	WE	1	4651477	69.31
108689	GAL	JE	7	2991314	32.36	111281	BBE	WE	1	2885720	47.31
108693	BBE	JE	1	1163353	23.30	111285	BBE	WE	43	4019806	72.93
108698	BBE	JE	1	1431383	27.25	111306	nas	WE	1	7423107	95.54
108701	BBE	JE	1	1207774	22.02	111326	YBE	JE	40	4854468	47.80
108710	YBE	JE	1	1318929	23.95	111335	PLB	JE	29	1332529	20.57
108847	nas	JE	13	1745471	25.49	111360	BBE	JE	29	2741849	28.97
108851	nas	JE	13	623732	15.22	111361	BBE	JE	29	5126766	76.29
110294	PLR	JE	25	643533	13.70	111363	PLB	JE	29	3482993	48.93
110296	nas	EA	1	1248435	20.55	111364	YBE	JE	29	3061378	44.35
110310	PLR	JE	25	1483749	27.93	111406	nas	WE	5	531023	10.59
110313	PLR	JE	25	848488	14.57	111411	YBE	WE	5	833898	14.85
110315	PLR	JE	25	649551	13.42	111412	nas	WE	5	530424	9.34
110320	PLR	EA	25	1183883	22.92	111413	YBE	WE	5	2855636	33.24
110339	nas	EA	1	644404	9.67	111431	nas	JE	3	1586534	24.36
110340	PLR	EA	25	1169859	21.89	111472	BBE	EA	5	4378006	64.26
110344	PLR	EA	25	1365536	27.37	111475	nas	EA	5	1119109	19.61
110346	PLR	EA	20	1440290	29.85	111477	nas	EA	5	2789061	48.30

Table S3: Phenotypic characteristics were used to define nine phenotypically different morphs of *Astatotilapia sp.* 'Chala'. The name of the morphs were chosen to be descriptive of a distinct feature of each morph. In most cases this is based on a specific colouration pattern, but could as well refer to features that reminded us of a different genera (*Gaurochromis* for GAL) or trophic guild (planktivore for PLR and PLB). Assignment to the different morphs was done by visual inspection of standardized pictures of live fish. 120 *Astatotilapia* from Lake Chala were assigned visually to a morph; the others could not be assigned because of shape distortion and/or loss of colour as a consequence of capture in gill nets.

Phenotype	Jaws	Overall shape	Stripes	Branchyostegal membrane	Belly	Flank	Shoulder patch	Operculum	N
Blue Belly (42)	Very slightly prognathous	Straight to decurved dorsal head profile	Mid- and dorsolateral	Sooty to black	sooty to black	Greenish to blue	None	Dark-blue to grey	22
Gaurochromis-Like (GAL)	Slightly prognathous	Deep dorsal head profile	Distinct vertical bars	black	black	-	None	-	16
Lean (LEA)	Long, lower jaw, slightly prognathous	Slender, front heavy	-	black	black	-	None	Grey to black	11
Lean orange (LEO)	Slightly prognathous	Slender, front heavy	-	sooty	sooty	yellow	Bright orange	Light	4
Large Mouth (LMO)	Long lower jaw, prognathous	Large	-	Blue-grey	Blue-grey	Yellowish or blue	None	Light blue	12
Orange Shoulder (OSH)	prognathous	Large, long and straight	-	yellow	yellow or black	Bright yellow	Orange	Light grey to yellowish	14
Blue Planktivore (PLB)	retrognathous	Slender	Many narrow vertical bars	black	Black	-	None	Grey to black	16
Red Planktivore (PLR)	retrognathous	-	Many narrow vertical bars	yellowish	Light	Yellow to pinkish	Faint orange	Light	10
Yellow Belly (YBE)	Very slightly prognathous	Slender, pointed	Midlateral, dorsolateral	yellow	Yellow	yellow to green	None	Light grey	15

Table S4: Definitions of the regions on the fish body where colour was scored in *Astatotilapia sp.* 'Chala'. The third column depicts which colours were present in the specified region and the fourth column depicts to which of the two colour morphs a colour was assigned.

Area	Definition	Colour				Assigned
Upper lip	Upper lip	Black	Blue	grey		**Blue (1)**
		brown	yellow	green		**Yellow (0)**
Lower lip	Lower lip	Blue	Black	grey		**Blue (1)**
		Beige	yellow	brown	green	**Yellow (0)**
Branchyo	Branchyostegal membrane	Blue	Black			**Blue (1)**
		White	yellow			**Yellow (0)**
Sub-operculum	Caudal ventral area on the operculum	Blue	Dark	black		**Blue (1)**
		Beige	yellow	brown	green	**Yellow (0)**
Belly	Region caudal of the branchyo-stegal membrane until the anus	Blue	Black			**Blue (1)**
		yellow	White	grey		**Yellow (0)**
Rostral dorsum	Region dorsal of the lateral line between the operculum and the anus	purple	Black	grey		**Blue (1)**
		copper	yellow	brown	orange	**Yellow (0)**
Caudal dorsum	Region dorsal of the lateral line from the beginning of the anal fin to the caudal fin	purple	Black	grey		**Blue (1)**
		copper	yellow	brown		**Yellow (0)**
Flank	Area between the caudal end of the pectoral fin and the caudal fin ventral of the lateral line	Blue	Green	grey	black	**Blue (1)**
		copper	yellow	beige	brown	**Yellow (0)**

Table S5: Tests of introgression. D statistics are used to compare levels of allele sharing between a taxon „P3" with each of two closely related groups ("P1" or "P2") using an outgroup to determine the ancestral allele. The overall genealogy is (((P1, P2), P3), O). In the absence of gene flow between P3 and either P1 or P2, P1 and P2 are expected to share equal amounts of derived alleles with P3 and the D statistics should be around 0. In the case of gene flow between P3 and P1, there is excess allele sharing between P3 and P1 relative to P2, rendering the D statistics positive. Here, positive D statistics with z-scores above 3 would indicate gene flow between *Astatotilapia* sp. 'Chala' (P1) and P3. Allele sharing between *A.* sp. 'Chala' (P1) and P3 is compared to allele sharing between P3 and either *A. bloyeti* or *A. sparsidens* (P2). *Metriaclima zebra* is used as outgroup to determine the ancestral allele.

P2	**P3**	**D statistic**	**z score**
Astatotilapia cf. bloyeti Pangani	Lake Victoria Region Superflock	0.08	1.35
Astatotilapia sparsidens	Lake Victoria Region Superflock	-0.0001	-0.001
Astatotilapia cf. bloyeti Pangani	*"Haplochromis" gracilior*	0.07	1.30
Astatotilapia sparsidens	*"Haplochromis" gracilior*	-0.06	-0.90
Astatotilapia cf. bloyeti Pangani	*Astatotilapia sparsidens*	0.10	1.99
Astatotilapia cf. bloyeti Pangani	*Astatotilapia cf. bloyeti* Ruaha	-0.25	-4.37

Table S6: Defined ranges and estimated parameters for the 16 demographic models that we tested. Italic entries represent priors for the models. The second column indicates whether a model assumed within Lake Chala constant population size (-), a bottleneck (b), expansion (e) or a bottleneck followed by an expansion (b+e). In the third column (2nd) it is indicated whether we modelled a second colonization event (1% of the ancestral population). NRI = Current effective population size of the riverine population, NLC = Current effective population size in Lake Chala, NPN = Current effective population size of *P. nyererei*, NPP = Current effective population size of *P. pundamilia,* NBOT = Effective population size in Lake Chala during the bottleneck, NRC = Effective population size of *Astatotilapia* before the colonization of Lake Chala, NPU = Effective population size of *Pundamilia* before speciating into *P. nyererei* and *P. pundamilia*, NANC = Effective ancestral population size before the split between *Astatotilapia* and *Pundamilia*, TANC = Split-time between *Astatotilapia* and *Pundamilia,* TPUN = Split-time between *P. nyererei* and *P. pundamilia,* TSPLIT = Colonization time of Lake Chala by *Astatotilapia*, TADM = Time of a second colonization event, TBOT = Time when the population in Lake Chala recovered from the bottleneck, GRO = Expansion rate per generation (negative values indicate population growth).

			Population size								**Split time**					**Expansion**	**Likelihood**	
			Riverine	**Lake Chala**	***P. nyererei***	***P. pundamilia***	**Bot**	**NRI+NLC**	**NPN+NPP**	**NRC+NPU**	**NPUvsNRC**	**NPNvsNPP**	**Col**	**2nd Col**	**Bot**	**Expansion**	**Estimated**	**Observed**
Parameter		**2nd**	**NRI**	**NLC**	**NPN**	**NPP**	**NBOT**	**NRC**	**NPU**	**NANC**	**TANC**	**TPUN**	**TSPLIT**	**TADM**	**TBOT**	**GRO**	**Est**	**Obs**
Search range	**min**		*1000*	*100*	*na*	*na*	*NLC*0.01*	*NRI*0.1*	*na*	*na*	*3000000*	*na*	*TANC*0.000001*	*TCHALA*0.0001*	*TCHALA*0.0001*	*-0.00005*	*na*	*na*
	max		*50000*	*10000*	*na*	*na*	*NLC*0.1*	*NRI*10*	*na*	*na*	*3000000*	*na*	*TANC*0.01*	*TCHALA*1*	*TCHALA*1*	*0*	*na*	*na*
Mutation rate models	-	no	38073	214	na	na	na	5075	na	na	na	na	105	na	na	na	-822.0	-778.5
	b	no	4324	391	na	na	4	445	na	na	na	na	21	na	19	na	-820.0	-778.5
	e	no	14314	141	na	na	na	2627	na	na	na	na	71	na	na	-0.000022	-821.8	-778.5
	b+e	no	31548	8467	na	na	95	5518	na	na	na	na	318	na	271	-0.0000084	-820.0	-778.5
	-	yes	56968	832	na	na	na	11379	na	na	na	na	464	0	na	na	-819.7	-778.5
	b	yes	3741	783	na	na	9	633	na	na	na	na	36	1	31	na	-817.6	-778.5
	e	yes	46403	1167	na	na	na	15370	na	na	na	na	682	3	na	-0.000041	-817.8	-778.5
	b+e	yes	44194	7127	na	na	111	11379	na	na	na	na	412	7	356	-0.000032	-817.5	-778.5
Search range	**min**		*1000*	*100*	*na*	*1000*	*NLC*0.01*	*NRI*0.1*	*na*	*NRC*0.1*	*Fixed*	*na*	*TANC*0.000001*	*TCHALA*0.0001*	*TCHALA*0.0001*	*-0.00005*	*na*	*na*
	max		*50000*	*10000*	*na*	*50000*	*NLC*0.1*	*NRI*10*	*na*	*NRC*100*	*Fixed*	*na*	*TANC*0.01*	*TCHALA*1*	*TCHALA*1*	*0*	*na*	*na*
Three population models	-	no	40346	172	na	584726	na	235105	Na	25418	3000000	na	40	na	na	na	-9679.9	-8571.6
	b	no	45019	4343	na	580304	55	228517	Na	28557	3000000	na	22	na	6	na	-9685.7	-8571.6
	e	no	36710	1587	na	580175	na	224498	Na	23657	3000000	na	570	na	na	-0.000043	-9683.2	-8571.6
	b+e	no	30873	5038	na	579940	101	205676	Na	35261	3000000	na	33	na	0	-0.000024	-9687.3	-8571.6
	-	yes	43607	1006	na	580315	na	214011	Na	30155	3000000	na	324	5	na	na	-9683	-8571.6
	b	yes	29553	8181	na	575957	61	227004	Na	23448	3000000	na	29	8	6	na	-9688.9	-8571.6
	e	yes	29091	495	na	578354	na	238712	Na	25221	3000000	na	203	5	na	-0.000019	-9686.2	-8571.6

	b+e	yes	33817	4301	na	578274	58	223351	Na	23292	3000000	na	20	0	0	-0.0000063	-9682	-8571.6
Search range	**min**		*1000*	*100*	*1000*	*1000*	*NLC*0.01*	*NRI*0.1*	*NPP*0.1*	*NRC*0.1*	*TPUN*1*	*Fixed*	*TPUN*0.001*	*TCHALA*0.01*	*TCHALA*0.01*	*-0.00005*	*na*	*na*
	max		*50000*	*10000*	*50000*	*50000*	*NLC*0.1*	*NRI*10*	*NPP*10*	*NRC*100*	*TPUN*100*	*Fixed*	*TPUN*1*	*TCHALA*1*	*TCHALA*1*	*0*	*na*	*na*
Four population models	-	no	6222	8186	43999	9191	na	2827	9161	38768	12493	6000	531	na	na	na	-15633.7	-15139.2
	b	no	16700	8077	27950	10305	500	3300	7903	42559	11751	6000	73	na	7	na	-15638.8	-15139.2
	e	no	5686	2186	16059	8689	na	1944	1461	24488	6890	6000	273	na	na	-0.000035	-15617.6	-15139.2
	b+e	no	3589	4047	4162	4430	79	1263	1929	14231	6000	6000	11	na	2	-0.00056	-15682.3	-15139.2
	-	yes	2304	5656	19684	8995	na	2714	5423	32365	10290	6000	255	73	na	na	-15624.1	-15139.2
	b	yes	5131	3359	4992	23422	224	2940	5140	24476	9992	6000	22	0	0	na	-15639	-15139.2
	e	yes	2335	6614	13670	11414	na	1753	2021	31005	7271	6000	409	75	na	-0.0000087	-15622.4	-15139.2
	b+e	yes	15028	1869	2675	5708	90	1627	1272	11771	6000	6000	9	0	0	-0.000033	-15694.2	-15139.2

Table S7: P-values of the differences in morphological traits (ANOVA) and the differences in trait variance (Levene test) between *Astatotilapia* from Lake Chala and from Nyumba ya Mungu. The last column (Permutation) indicates the ratio of how often the range of the trait values in ten subsampled individuals of Lake Chala exceeded the trait range observed in the ten individuals from Nyumba ya Mungu. Significant P-values after sequential Bonferroni correction are highlighted in bold.

	ANOVA	Levene	Permutation
HL	0.1173	0.2740	0.348
HW	**<0.0001**	0.0629	0.884
BD	**0.0003**	0.2428	0.876
LJL	0.0812	0.2794	0.757
LJW	**<0.0001**	0.2929	0.124
SnL	**0.0015**	0.5801	0.142
SnW	0.1553	0.9556	0.357
ChD	0.6955	0.4653	0.493
POD	0.0194	0.4147	0.163
IOW	**<0.0001**	0.9792	0.499
EyL	**<0.0001**	0.5410	0.655
EyD	**<0.0001**	0.5127	0.454
POW	**0.0004**	0.4964	0.768
PPL	0.1478	**0.0004**	0.003

Table S8: Results of the ANOVAs testing for correlations between univariate morphological traits and ecology ("phenotype-environment correlations"). P-values below 0.05 are indicated in bold, asterisks indicate significance after sequential Bonferroni correction (* < 0.05, ** < 0.01, *** < 0.001). Superscripts at the F-value indicate positive (p) or negative (n) correlations. For depth, a positive correlation means that the trait is bigger in fish caught at deeper depth.

	Depth		dC13		dN15	
Trait	F	P	F	P	F	P
HL	0.0049	0.9442	0.3915	0.5326	0.6932	0.4066
HW	13.53^{n}	**0.000283*** **	0.121	0.7285	1.4297	0.234
BD	5.3171^{n}	**0.02187**	0.0224	0.8812	1.4969	0.2233
LJL	0.4764	0.4906	9.2477^{n}	**0.002848***	0.1151	0.735
LJW	6.905^{n}	**0.009083**	2.4866	0.1172	0.8816	0.3495
SnL	0.1006	0.7514	5.5811^{p}	**0.01963**	0.3406	0.5605
SnW	18.04^{n}	**0.0000297****	0.0665	0.7969	0.9675	0.3271
ChD	5.0807^{n}	**0.02499**	4.9672^{n}	**0.02754**	1.7208	0.1919
POD	0.0066	0.9353	0.0186	0.8917	0.1215	0.728
IOW	0.3135	0.576	5.4069^{n}	**0.02159**	2.5681	0.1114
EyL	0.1259	0.723	0.0003	0.9867	14.878^{n}	**0.0001791****
EyD	0.4291	0.513	0.5135	0.4749	14.263^{n}	**0.0002402****
POW	13.018^{n}	**0.000367****	0.0469	0.8289	1.3131	0.2539
PPL	2.4193	0.121	0.4322	0.5121	6.433^{n}	**0.01238**

Table S9: Bhattacharyya distances calculated from morphology (LD1 and LD2) between phenotypes (lower left) and the corresponding P-values before sequential Bonferroni correction (upper right). Bold values indicate significance before sequential Bonferroni correction and asterisks indicate significance level after sequential Bonferroni correction (* < 0.05, ** < 0.01, ** < 0.001).

	BBE	GAL	LEA	LEO	LMO	OSH	PLB	PLR	YBE
BBE		<0.001	0.558	0.102	0.080	<0.001	0.391	0.045	0.007
GAL	**0.464*** **		<0.001	0.001	0.001	<0.001	<0.001	0.052	0.001
LEA	0.165	**0.929*** **		0.055	0.021	<0.001	0.127	0.009	0.023
LEO	0.827	**2.235***	**0.812**		0.040	0.005	0.061	0.023	0.055
LMO	0.108	**0.376***	**0.457**	**1.126**		<0.001	0.223	0.350	<0.001
OSH	**0.517*** **	**0.557*** **	**0.647*** **	**1.476**	**0.995*** **		<0.001	<0.001	0.080
PLB	0.030	**0.597*** **	0.223	0.867	0.083	**0.883*** **		0.051	<0.001
PLR	**0.170**	**0.165**	**0.503**	**1.363**	0.088	**0.992*** **	**0.173**		0.001
YBE	**0.207**	**0.298***	**0.343**	1.079	**0.482*** **	0.111	**0.416*** **	**0.404***	

Table S10: Loadings on the first eight axes of the LDA based on morphological traits. Values above 0.3 in the first two axes are indicated in bold.

	LD1	LD2	LD3	LD4	LD5	LD6	LD7	LD8
HL	**-0.396**	0.190	0.033	0.060	-0.370	0.502	-0.574	0.521
HW	**-1.195**	-0.233	-0.409	0.133	0.284	-0.335	-0.362	-0.270
BD	**0.759**	**-1.017**	0.551	0.336	-0.586	0.567	0.577	0.041
LJL	**0.858**	**0.356**	0.146	0.096	0.363	-0.753	-0.370	-0.068
LJW	-0.213	-0.149	-0.081	-0.112	0.887	0.130	0.372	-0.450
SnL	**0.462**	-0.292	-0.629	-0.900	-0.329	-0.378	0.355	-0.387
SnW	-0.184	**0.640**	1.177	-0.193	-0.646	-0.872	-0.065	-0.138
ChD	-0.113	-0.145	-0.294	0.368	0.146	-0.267	0.241	0.691
POD	0.042	**0.390**	0.012	0.021	0.524	0.386	0.297	0.272
IOW	**-0.314**	**-0.394**	-0.020	-0.232	-0.295	-0.635	0.116	-0.230
EyL	0.109	0.043	-0.656	0.466	0.172	-0.041	-0.117	-0.729
EyD	**0.311**	**-0.331**	-0.225	-0.213	0.144	0.224	0.211	0.392
POW	0.286	**-0.339**	-0.556	-0.452	0.652	0.840	-0.634	0.546
PPL	-0.133	0.291	-0.001	0.219	-0.115	0.034	-0.081	0.453

Table S11: Schoener's (1970) index of overlap for prey items. Values below 40% (indicated in bold) are considered to be differentiated prey compositions. Sample sizes are indicated in parentheses.

Schoener's index	BBE	GAL	LEA	LMO	OSH	PLB	PLR	YBE
BBE (14)								
GAL (7)	0.57							
LEA (5)	0.65214	**0.382**						
LMO (8)	0.54241	0.58893	0.54638					
OSH (10)	0.63886	0.68657	0.485	0.59163				
PLB (5)	0.52886	0.43671	0.717	0.535	0.54			
PLR (3)	0.41738	**0.2733**	0.71533	**0.37**	**0.375**	0.775		
YBE (10)	0.64314	0.562	0.711	0.55188	0.558	0.64	0.49633	
NYM (6)	**0.3586**	**0.2471**	0.41571	**0.347**	**0.3426**	0.50271	0.43905	**0.2507**

Table S12: Bhattacharyya distances calculated from stable isotopes ($\delta^{13}C$ and $\delta^{15}N$) between phenotypes (lower left) and the corresponding P-values (upper right). Asterisks and bold indicate significant Bhattacharyya distance after sequential Bonferroni correction (* < 0.05, ** < 0.01, ** < 0.001).

	BBE	GAL	LEA	LEO	LMO	OSH	PLB	PLR	YBE
BBE		0.595	0.655	0.775	0.326	0.158	0.023	0.699	0.502
GAL	0.405		0.595	0.800	0.185	0.020	0.003	0.013	0.019
LEA	0.173	0.137		0.771	0.088	0.009	0.055	0.086	0.098
LEO	2.397	1.604	1.982		0.338	0.019	0.205	0.119	0.222
LMO	0.252	0.141	0.173	2.063		0.739	0.001	0.125	0.085
OSH	0.785	0.458	0.762	2.394	0.325		<0.001	0.043	0.054
PLB	0.561	0.634	0.457	2.526	**0.739***	**1.536****		<0.001	0.001
PLR	0.231	0.361	0.209	2.405	0.140	0.550	**1.167***		0.719
YBE	0.059	0.484	0.264	2.551	0.265	0.766	**0.829***	0.164	

Table S13: Pairwise genomic differentiation between the different morphs if aligned to the reference genome of *Metriaclima zebra* (above diagonal) and *Oreochromis niloticus* (below diagonal). The reported F_{ST}s represent the average pairwise F_{ST} for 50 subsampling-events of N-1 genotypes per morph, where N represents the sample size in the less abundant morph of the pairwise comparison (e.g. F_{ST} between BBE and LEA is based on 50 subsampling event of 4 genotypes per morph (N_{LEA} = 5)). Highest genomic divergence is found for GAL and PLR. F_{ST}s higher than expected by chance are indicated in bold. Three pairwise comparisons are significant for both alignments: GAL/LMO, GAL/PLR and GAL/YBE.

	N	BBE	GAL	LEA	LMO	OSH	PLB	PLR	YBE
BBE	14		0.003	0.007	-0.002	-0.007	0.004	0.000	-0.004
GAL	12	0.004		0.009	**0.004**	0.003	**0.011**	**0.013**	**0.005**
LEA	5	0.013	0.009		-0.002	-0.006	0.001	**0.015**	0.004
LMO	12	-0.006	**0.006**	0.002		-0.004	0.007	**0.007**	-0.001
OSH	4	-0.001	0.000	-0.003	-0.008		-0.007	0.005	-0.003
PLB	6	0.004	0.012	0.008	0.002	-0.005		**0.019**	0.004
PLR	9	-0.006	**0.010**	0.003	-0.001	0.001	0.011		**0.007**
YBE	12	0.003	**0.010**	0.003	0.001	0.001	0.005	0.004	

Table S14: Linear selection gradients and matrix of quadratic and correlational selection gradients of the 14 morphological traits calculated with the methods from Lande and Arnold (20). Significant selection gradients are indicated in bold. Superscripts indicate s = stabilizing or d = directional selection. No evidence of disruptive selection was found.

	B	HL	HW	BD	LJL	LJW	SnL	SnW	ChD	POD	IOW	EyL	EyD	POW	PPL
HL	-0.02	-0.26													
HW	-0.03	-0.01	0.31												
BD	-0.05	-0.25	0.08	-0.28											
LJL	0.02	-0.11	-0.00	0.28	0.06										
LJW	0.08	**0.45^{s}**	0.03	0.07	-0.19	-0.42									
SnL	0.14	-0.83	-0.22	-0.11	0.42	-0.21	0.11								
SnW	-0.19	-0.08	-0.19	0.25	-0.09	0.29	-0.21	0.39							
ChD	0.07	**0.48^{s}**	**-0.35^{s}**	0.11	-0.12	0.00	0.17	0.02	-0.32						
POD	-0.01	-0.42	-0.13	0.17	0.13	-0.05	-0.12	-0.26	-0.09	-0.01					
IOW	-0.05	0.09	0.06	-0.12	-0.39	-0.13	0.01	0.80	-0.21	0.10	-0.39				
EyL	0.00	**0.53^{s}**	0.32	-0.09	0.16	-0.09	-0.57	**-0.49^{d}**	010	0.21	-0.07	-0.59			
EyD	-0.06	-0.40	-0.04	0.08	-0.14	-0.11	0.61	-0.53	0.00	0.30	0.13	-0.91	-0.08		
POW	0.12	0.58	0.20	0.08	-0.09	-0.20	0.07	0.26	0.12	0.07	-0.10	**-0.16^{d}**	-0.25	0.44	
PPL	-0.01	0.15	0.10	-0.16	0.25	-0.01	-0.02	0.04	0.20	-0.01	0.41	-0.01	-0.11	0.45	-0.05

Table S15: Eigen matrix of eigenvectors for the canonical analysis. Eigenvectors > 0.3 and < -0.3, and significant selection gradients are indicated in bold. Negative γ indicates stabilizing selection, whereas positive γ indicates disruptive selection. No significant evidence for disruptive selection was found.

	Λ	HL	HW	BD	LJL	LJW	SnL	SnW	ChD	POD	IOW	EyL	EyD	POW	PPL	β	Γ
M1	2.21	**0.32**	**0.47**	0.03	-0.14	-0.01	0.25	0.04	-0.30	**-0.34**	**-0.38**	-0.05	-0.05	-0.06	**-0.48**	0.43	0.43
M2	0.96	0.09	0.05	0.29	**0.75**	-0.26	0.24	0.21	-0.10	0.05	0.30	-0.09	-0.06	-0.23	-0.10	-0.25	-0.16
M3	0.80	-0.02	-0.29	-0.01	-0.08	-0.17	**0.41**	**0.36**	-0.20	**0.31**	-0.18	**0.53**	0.12	**0.33**	-0.09	-0.12	-0.06
M4	0.63	-0.15	-0.29	-0.23	-0.04	**-0.61**	-0.20	0.18	-0.25	**-0.31**	-0.26	-0.18	**-0.31**	-0.10	0.18	-0.21	0.08
M5	0.36	0.04	0.29	0.00	-0.19	-0.07	0.22	**0.47**	0.20	0.21	0.06	**-0.58**	-0.05	**0.37**	0.22	**0.24**	0.04
M6	-0.01	**-0.34**	-0.17	-0.22	-0.04	0.23	**0.63**	-0.20	**-0.32**	-0.21	0.12	-0.26	0.17	-0.14	0.19	0.30	-0.03
M7	-0.04	**-0.56**	0.22	**-0.42**	0.18	0.02	-0.18	0.29	0.13	0.08	-0.10	-0.02	**0.32**	-0.13	**-0.39**	-0.14	-0.02
M8	-0.08	0.10	0.22	-0.10	**-0.40**	0.00	-0.08	**0.37**	-0.26	0.07	**0.49**	0.24	-0.02	**-0.49**	0.15	**-0.43**	0.06
M9	-0.19	0.04	**-0.41**	0.06	0.02	**0.55**	0.04	**0.44**	0.20	-0.13	-0.18	-0.07	**-0.38**	-0.24	-0.16	0.01	-0.06
M10	-0.66	0.05	-0.04	-0.03	0.04	-0.01	-0.01	0.22	0.22	**-0.74**	**0.36**	0.20	0.21	**0.37**	0.00	0.16	-0.22
M11	-0.70	-0.26	**0.33**	**0.35**	0.17	0.21	-0.10	0.19	-0.13	-0.15	**-0.40**	0.22	0.10	-0.04	**0.57**	**-0.28**	**-0.09**
M12	-0.82	-0.06	-0.29	**0.47**	-0.16	0.07	**-0.32**	0.13	**-0.43**	0.01	0.07	**-0.32**	**0.43**	0.09	-0.23	0.14	-0.03
M13	-1.00	**0.58**	-0.16	**-0.37**	0.19	0.05	-0.06	0.11	0.03	0.03	-0.23	-0.11	**0.52**	-0.18	0.25	-0.29	**-0.37**
M14	-2.49	0.09	0.09	**-0.37**	**0.30**	**0.34**	-0.26	0.03	**-0.53**	0.08	0.15	0.00	-0.29	**0.42**	0.03	0.53	**-0.34**

Table S16: Eigenvectors of the PPR analysis on all depth ranges combined (All) and on the three different depth categories. Eigenvectors > 0.3 and < -0.3 of the axes with one or two fitness optima are indicated in bold. Traits with high eigenvectors on axes under disruptive selection within more than one depth range are underlined

	All		**Shallow**		**Intermediate**		**Deep**	
	a1	**a2**	**a1**	**a2**	**a1**	**a2**	**a1**	**a2**
# optima	**two**	**one**	**two**	**one**	**one**	**two**	**two**	**one**
HL	-0.20	0.17	**-0.36**	**0.53**	-0.09	**0.32**	**0.44**	**0.48**
HW	-0.27	0.17	-0.11	-0.16	**0.37**	-0.11	0.10	**-0.62**
BD	-0.22	-0.11	-0.16	0.11	-0.16	-0.29	**-0.38**	-0.03
LJL	-0.15	**0.37**	0.22	0.04	**-0.57**	0.10	0.23	0.07
LJW	0.20	-0.04	0.11	-0.20	0.27	0.09	**0.36**	-0.11
SnL	**0.69**	**-0.33**	**0.54**	-0.12	0.23	**-0.32**	-0.06	-0.09
SnW	-0.28	**-0.39**	**-0.51**	-0.19	-0.29	**0.51**	-0.20	-0.06
ChD	**0.36**	-0.15	0.14	-0.09	0.18	0.21	0.20	0.13
POD	-0.14	0.27	-0.15	**0.46**	-0.05	0.09	-0.21	**0.45**
IOW	0.05	**-0.44**	0.02	-0.19	-0.27	-0.23	-0.10	-0.12
EyL	0.13	-0.10	-0.01	0.20	0.26	0.01	0.13	0.00
EyD	-0.12	-0.20	-0.02	-0.06	**-0.30**	**-0.41**	**-0.38**	0.07
POW	0.11	**0.35**	**0.39**	**0.50**	-0.05	**-0.38**	-0.07	**0.30**
PPL	-0.17	0.25	-0.17	0.18	0.12	0.09	**-0.41**	-0.14

Table S17: Linear and quadratic selection coefficients (β, γ) and AICc values of the different regressions on the PPR analysis axes. Significant coefficients and AICc values of the best significant polynomial models are depicted with asterisks (° < 0.1, * < 0.05, ** < 0.01, ** < 0.001) and in bold respectively.

				AICc of the polynomial models				
		β	Γ	1st	2nd	3rd	4th	5th
All (N=231)	**a1**	0.260	0.211	656.4*	653.5**	653.4*	655.5	**646.3*** **
	a2	0.155	-0.216	662.3	662.0	664.1	**658.8***	660.3°
Shallow (N=84)	**a1**	0.743	0.826	266.5*	266.2*	262.1**	264.3**	**256.2*** **
	a2	0.185	-0.104	271.8	272.6	268.1*	269.4°	**264.0****
Intermediate (N=70)	**a1**	0.259	-0.508	195.2*	188.6**	**185.6*** **	188.0**	187.4**
	a2	0.256	0.139	196.9°	199.1	201.2	202.4	**187.5****
Deep (N=77)	**a1**	0.343	0.480	185.2**	183.0**	**179.4****	180.5**	181.0**
	a2	0.026	-0.367	192.0	183.1**	183.6**	**169.2*** **	169.9***

Table S18: Significance levels of relative occurrence of the different morphs at the two peaks along the axes of strongest disruptive selection. Significant values are indicated in bold. Values > 0.95 indicate significantly less abundant than expected by chance, whereas values < 0.05 indicate significantly more abundant than expected by chance. Morphs that were present with less than four individuals in a depth category were excluded (-).

	All		Shallow		Intermediate		Deep	
Peak at	**high a1**	**low a1**	**high a1**	**low a1**	**high a2**	**low a2**	**high a1**	**low a1**
BBE	0.17	0.936	0.662	0.315	-	-	0.174	0.949
GAL	**>0.999**	**<0.001**	**>0.999**	**<0.001**	-	-	-	-
LEA	**0.975**	0.095	-	-	0.839	0.488	0.322	**>0.999**
LEO	0.341	**>0.999**	-	-	-	-	-	-
LMO	0.879	0.569	0.795	0.166	-	-	-	-
OSH	0.311	0.916	0.405	**>0.999**	0.54	0.89	-	-
PLB	0.444	0.645	-	-	-	-	0.688	0.548
PLR	0.558	0.787	-	-	**0.039**	**0.994**	-	-
YBE	0.896	0.133	0.364	0.568	-	-	-	-

References:

1. Conte MA, Kocher TD. An improved genome reference for the African cichlid, Metriaclima zebra. Bmc Genomics. 2015;16.
2. Conte MA, Gammerdinger WJ, Bartie KL, Penman DJ, Kocher TD. A high quality assembly of the Nile Tilapia (Oreochromis niloticus) genome reveals the structure of two sex determination regions. Bmc Genomics. 2017;18.
3. Marques DA, Lucek K, Meier JI, Mwaiko S, Wagner CE, Excoffier L, et al. Genomics of Rapid Incipient Speciation in Sympatric Threespine Stickleback. Plos Genet. 2016;12(2).
4. Danecek P, Auton A, Abecasis G, Albers CA, Banks E, DePristo MA, et al. The variant call format and VCFtools. Bioinformatics. 2011;27(15):2156-8.
5. Stamatakis A. RAxML version 8: a tool for phylogenetic analysis and post-analysis of large phylogenies. Bioinformatics. 2014;30(9):1312-3.
6. Willing EM, Dreyer C, van Oosterhout C. Estimates of Genetic Differentiation Measured by F-ST Do Not Necessarily Require Large Sample Sizes When Using Many SNP Markers. Plos One. 2012;7(8).
7. Excoffier L, Laval G, Schneider S. Arlequin (version 3.0): An integrated software package for population genetics data analysis. Evol Bioinform. 2005;1:47-50.
8. Excoffier L, Foll M. fastsimcoal: a continuous-time coalescent simulator of genomic diversity under arbitrarily complex evolutionary scenarios. Bioinformatics. 2011;27(9):1332-4.
9. Malinsky M, Svardal H, Tyers AM, Miska EA, Genner MJ, Turner GF, et al. Whole Genome Sequences Of Malawi Cichlids Reveal Multiple Radiations Interconnected By Gene Flow. bioRxiv. 2017.
10. Meier JI, Marques DA, Mwaiko S, Wagner CE, Excoffier L, Seehausen O. Ancient hybridization fuels rapid cichlid fish adaptive radiations. Nat Commun. 2017;8.
11. Patterson N, Moorjani P, Luo YT, Mallick S, Rohland N, Zhan YP, et al. Ancient Admixture in Human History. Genetics. 2012;192(3):1065-+.
12. Selz OM, Thommen R, Maan ME, Seehausen O. Behavioural isolation may facilitate homoploid hybrid speciation in cichlid fish. J Evolution Biol. 2014;27(2):275-89.
13. Kishe-Machumu M, Witte F, Wanink JH. Dietary shift in benthivorous cichlids after the ecological changes in Lake Victoria. Anim Biol. 2008;58(4):401-17.
14. Szedlmayer ST, Able KW, Musick JA, Weinstein MP. Are Scale Circuli deposited daily in juvenile Weakfish, Cynoscion regalis. Environ Biol Fish. 1991;31(1):87-94.
15. Kingsford MJ, Atkinson MH. Increments in otoliths and scales - how they relate to the Age and early Development of reared and wild larval and juvenile Pagrus auratus (Sparidae). Australian Journal of Marine and Freshwater Research. 1994;45(6):1007-21.
16. Yamada J. Studies on the structure and growth of the scales in the goldfish: Hokkaido University; 1961.
17. Sire JY. Ontogenic Development of Surface Ornamentation in the Scales of Hemichromis-Bimaculatus (Cichlidae). J Fish Biol. 1986;28(6):713-24.
18. Rohlf FJ. The tps series of software. Hystrix. 2015;26(1):9-12.
19. Van Rijssel JC, Moser FN, DFrei D, Seehausen O. Prevalence of disruptive selection predicts extent of species differentiation in Lake Victoria cichlids. P Roy Soc B-Biol Sci. 2018;285(1871).
20. Lande R, Arnold SJ. The Measurement of Selection on Correlated Characters. Evolution. 1983;37(6):1210-26.
21. Akaike H. New Look at Statistical-Model Identification. Ieee T Automat Contr. 1974;Ac19(6):716-23.
22. Damste JSS, Ossebaar J, Abbas B, Schouten S, Verschuren D. Fluxes and distribution of tetraether lipids in an equatorial African lake: Constraints on the application of the TEX86 palaeothermometer and BIT index in lacustrine settings. Geochim Cosmochim Ac. 2009;73(14):4232-49.
23. Wood SN. Generalized Additive Models: An Introduction with R. Hall/CRC Ca, editor2017.

24. Moser FN, Van Rijssel JC, Ngatunga BP, Mwaiko S, Seehausen O. The origin and future of an endangered crater lake endemic; phylogeography and ecology of Oreochromis hunteri and its invasive relatives. Hydrobiologia. submitted.
25. Trewavas E. Tilapiine fishes of the genera Sarotherodon, Oreochromis and Danakilia. London: Brit. Mus. (Nat. Hist.)

1983.
26. Nagl S, Tichy H, Mayer WE, Samonte IE, McAndrew BJ, Klein J. Classification and phylogenetic relationships of African tilapiine fishes inferred from mitochondrial DNA sequences. Mol Phylogenet Evol. 2001;20(3):361-74.
27. Dadzie S, Haller RD, Trwavas E. A Note on the Fishes of Lake Jipe and Lake Chale on the Kenya-Tanzania Border. 1988.
28. Lowe RH. New species of Tilapia (Pisces, Cichlidae) from Lake Jipe and the Pangani River in East Africa. Bulletin of British Mueseum (Natural History). 1955;2:19.
29. Hermann CM, Sefc KM, Koblmuller S. Ancient origin and recent divergence of a haplochromine cichlid lineage from isolated water bodies in the East African Rift system. J Fish Biol. 2011;79(5):1356-69.
30. Seegers L, De Vos L, Okeyo DO. Annotated Checklist of the Freshwater Fishes of Kenya (excluding the lacustrine haplochromines from Lake Victoria). Journal of East African Natural History. 2003;92(11-47).
31. Seehausen O, Lippitsch E, Bouton N, Zwennes H. Mbipi, the rock-dwelling cichlids of Lake Victoria: description of three new genera and fifteen new species In: Kottelat M, editor. Ichthyological Exploration of Freshwaters: An international journal for field-oriented ichthyology. 9. München, Germany: Verlag Dr. Friedrich Pfeil; 1998.
32. Friedman ST, Price SA, Hoey AS, Wainwright PC. Ecomorphological convergence in planktivorous surgeonfishes. J Evolution Biol. 2016;29(5):965-78.
33. Schmitz L, Wainwright PC. Ecomorphology of the eyes and skull in zooplanktivorous labrid fishes. Coral Reefs. 2011;30(2):415-28.
34. van Rijssel JC, Hoogwater ES, Kishe-Machumu MA, van Reenen E, Spits KV, van der Stelt RC, et al. Fast adaptive responses in the oral jaw of Lake Victoria cichlids. Evolution. 2015;69(1):179-89.
35. Mcphail JD. Ecology and Evolution of Sympatric Sticklebacks (Gasterosteus) - Morphological and Genetic-Evidence for a Species Pair in Enos Lake, British-Columbia. Can J Zool. 1984;62(7):1402-8.
36. Ostbye K, Amundsen PA, Bernatchez L, Klemetsen A, Knudsen R, Kristoffersen R, et al. Parallel evolution of ecomorphological traits in the European whitefish Coregonus lavaretus (L.) species complex during postglacial times. Mol Ecol. 2006;15(13):3983-4001.
37. Malinsky M, Challis RJ, Tyers AM, Schiffels S, Terai Y, Ngatunga BP, et al. Genomic islands of speciation separate cichlid ecomorphs in an East African crater lake. Science. 2015;350(6267):1493-8.
38. Kautt AF, Machado-Schiaffino G, Torres-Dowdall J, Meyer A. Incipient sympatric speciation in Midas cichlid fish from the youngest and one of the smallest crater lakes in Nicaragua due to differential use of the benthic and limnetic habitats? Ecology and Evolution. 2016;6(15):5342-57.
39. Barel CDN, Van Oijen MJP, Witte F, Wittemaas ELM. Introduction to Taxonomy and Morphology of Haplochromine Cichlidae from Lake Victoria - Manual to Greenwoods Revision Papers. Neth J Zool. 1977;27(4):333-+.
40. Meier JI, Sousa VC, Marques DA, Selz OM, Wagner CE, Excoffier L, et al. Demographic modelling with whole-genome data reveals parallel origin of similar Pundamilia cichlid species after hybridization. Mol Ecol. 2017;26(1):123-41.
41. Kinaro ZO, Xue LY, Volatiana JA. Complete mitochondrial DNA sequences of the Victoria tilapia (Oreochromis variabilis) and Redbelly Tilapia (Tilapia zilli): genome characterization and phylogeny analysis. Mitochondr DNA. 2016;27(4):2455-7.
42. Coleman AT, Wibbels T, Huang Y-h, Marion K, Dindo J. Do larger females produce more fit hatchlings? Effect of female age and size on egg size and hatchling growth in the Mississippi diamondback terrapin, Malaclemys terrapin pileata. Integr Comp Biol. 2010;50:E31-E.